On the Use of Displacements in Data Assimilation

Yann MICHEL

Météo-France/CNRM/GMAP
NCAR seminar

11th November 2010

Second version including minor corrections and full bibliography

Purpose

Much of the work described in these slides is preliminary, which explains the extended bibliography and the brief review included on alignment data assimilation procedures and spatial correlation modeling.

The main concept around this work is the use of spatial deformations, either for data assimilation algorithm or for background error modeling in variationnal data assimilation. For data assimilation, the ultimate goal is to smoothly distord background fields to match observations of coherent structures. For background error modeling, the goal is to set flow-dependent, anisotropic and inhomogeneous correlation structures.

Both topic are of great interest for Météo-France and NCAR, and their better understanding was the purpose of my stay at NCAR.

Shortly, spatial deformation may be useful in correlation modeling, and optical flow and alignment data assimilation may use correlation modeling concepts.

Questions or comments may be adressed to `yann.michel@meteo.fr`

Let I be a sequence of images on a bounded domain $\Omega \subset \mathcal{R}^2$.
The Optical Flow [Horn and Schunck 1981] is the velocity field $\mathbf{v}$ verifying:

$$I(\mathbf{s} + \mathbf{v}\Delta_t, t + \Delta_t) \approx I(\mathbf{s}, t)$$

Motion estimation is part of most video coding schemes because it enables us to exploit the high degree of temporal redundancy present.

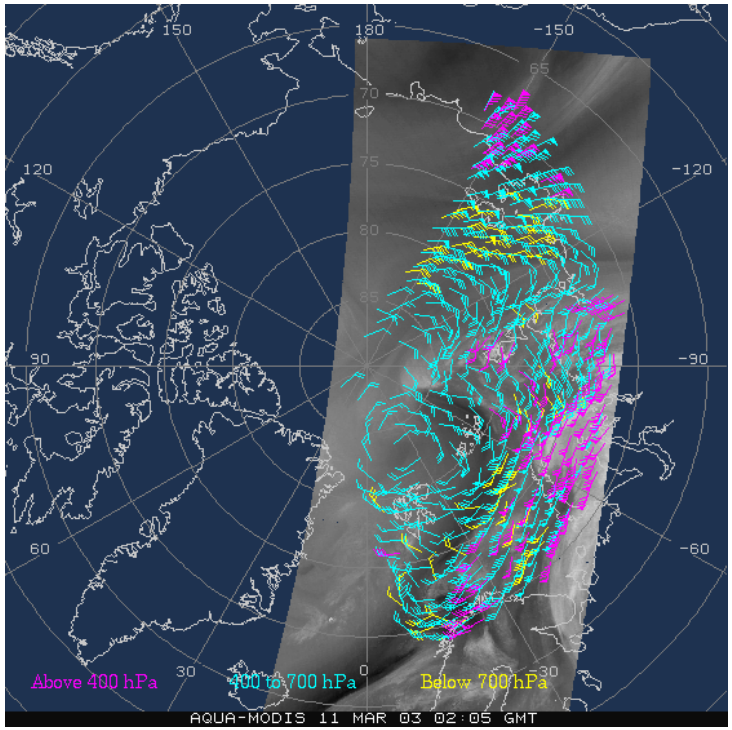

So far, Optical Flow techniques have been used on the observation side, for the purpose of deriving wind vectors by tracking features in IR/WV bands.

[Bormann et al. 2003] have shown that wind vectors have observation errors spatially correlated.

← Figure: AVHRR/MODIS Polar Wind vectors. Product from NOAA/NESDIS.

Let I be a sequence of images on a bounded domain $\Omega \subset \mathcal{R}^2$.
The Optical Flow [Horn and Schunck 1981] is the velocity field $\mathbf{v}$ verifying:

$$I(\mathbf{s} + \mathbf{v}\Delta_t, t + \Delta_t) \approx I(\mathbf{s}, t)$$

Motion estimation is part of most video coding schemes because it enables us to exploit the high degree of temporal redundancy present.

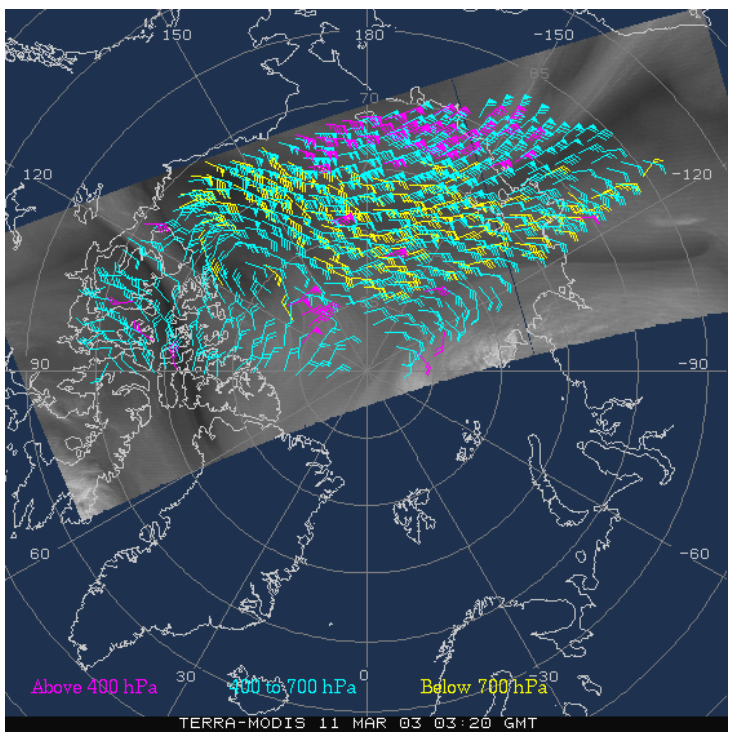

So far, Optical Flow techniques have been used on the observation side, for the purpose of deriving wind vectors by tracking features in IR/WV bands.

[Bormann et al. 2003] have shown that wind vectors have observation errors spatially correlated.

← Figure: AVHRR/MODIS Polar Wind vectors. Product from NOAA/NESDIS.

Let I be a sequence of images on a bounded domain $\Omega \subset \mathcal{R}^2$.
The Optical Flow [Horn and Schunck 1981] is the velocity field $\mathbf{v}$ verifying:

$$I(\mathbf{s} + \mathbf{v}\Delta_t, t + \Delta_t) \approx I(\mathbf{s}, t)$$

Motion estimation is part of most video coding schemes because it enables us to exploit the high degree of temporal redundancy present.

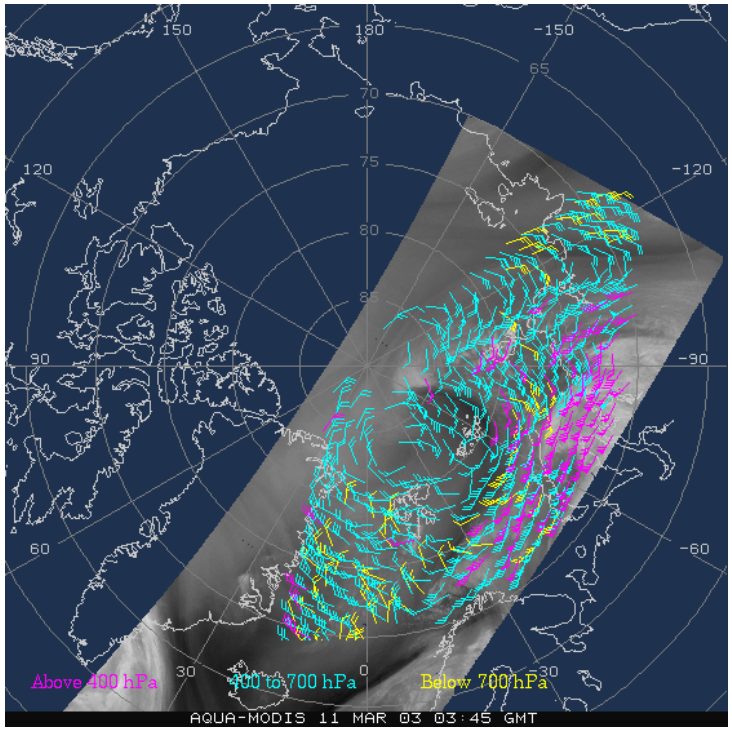

So far, Optical Flow techniques have been used on the observation side, for the purpose of deriving wind vectors by tracking features in IR/WV bands.

[Bormann et al. 2003] have shown that wind vectors have observation errors spatially correlated.

← Figure: AVHRR/MODIS Polar Wind vectors. Product from NOAA/NESDIS.

Let I be a sequence of images on a bounded domain $\Omega \subset \mathcal{R}^2$.
The Optical Flow [Horn and Schunck 1981] is the velocity field $\mathbf{v}$ verifying:

$$I(\mathbf{s} + \mathbf{v}\Delta_t, t + \Delta_t) \approx I(\mathbf{s}, t)$$

Motion estimation is part of most video coding schemes because it enables us to exploit the high degree of temporal redundancy present.

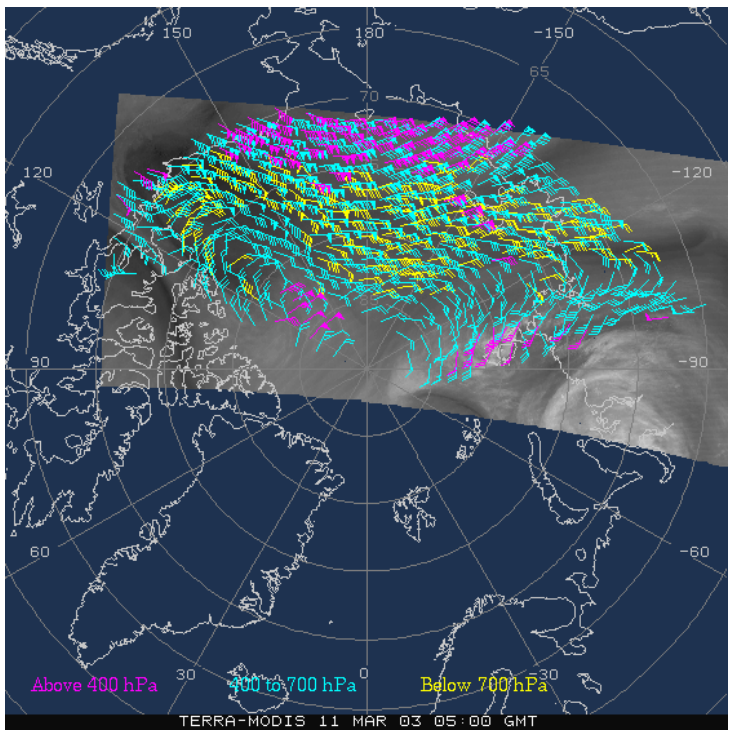

So far, Optical Flow techniques have been used on the observation side, for the purpose of deriving wind vectors by tracking features in IR/WV bands.

[Bormann et al. 2003] have shown that wind vectors have observation errors spatially correlated.

← Figure: AVHRR/MODIS Polar Wind vectors. Product from NOAA/NESDIS.

Let I be a sequence of images on a bounded domain $\Omega \subset \mathcal{R}^2$.
The Optical Flow [Horn and Schunck 1981] is the velocity field $\mathbf{v}$ verifying:

$$I(\mathbf{s} + \mathbf{v}\Delta_t, t + \Delta_t) \approx I(\mathbf{s}, t)$$

Motion estimation is part of most video coding schemes because it enables us to exploit the high degree of temporal redundancy present.

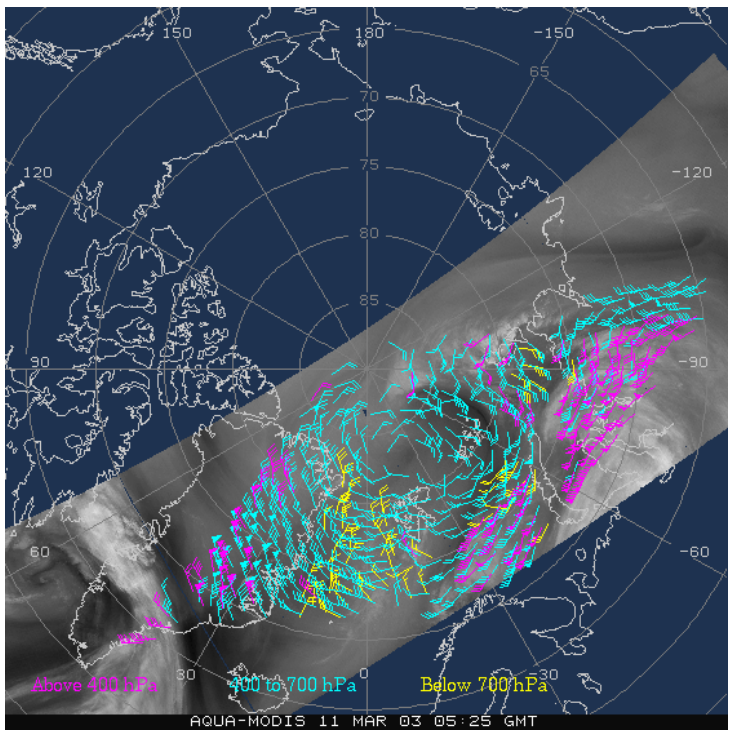

So far, Optical Flow techniques have been used on the observation side, for the purpose of deriving wind vectors by tracking features in IR/WV bands.

[Bormann et al. 2003] have shown that wind vectors have observation errors spatially correlated.

← Figure: AVHRR/MODIS Polar Wind vectors. Product from NOAA/NESDIS.

Let I be a sequence of images on a bounded domain $\Omega \subset \mathcal{R}^2$.
The Optical Flow [Horn and Schunck 1981] is the velocity field $\mathbf{v}$ verifying:

$$I(\mathbf{s} + \mathbf{v}\Delta_t, t + \Delta_t) \approx I(\mathbf{s}, t)$$

Motion estimation is part of most video coding schemes because it enables us to exploit the high degree of temporal redundancy present.

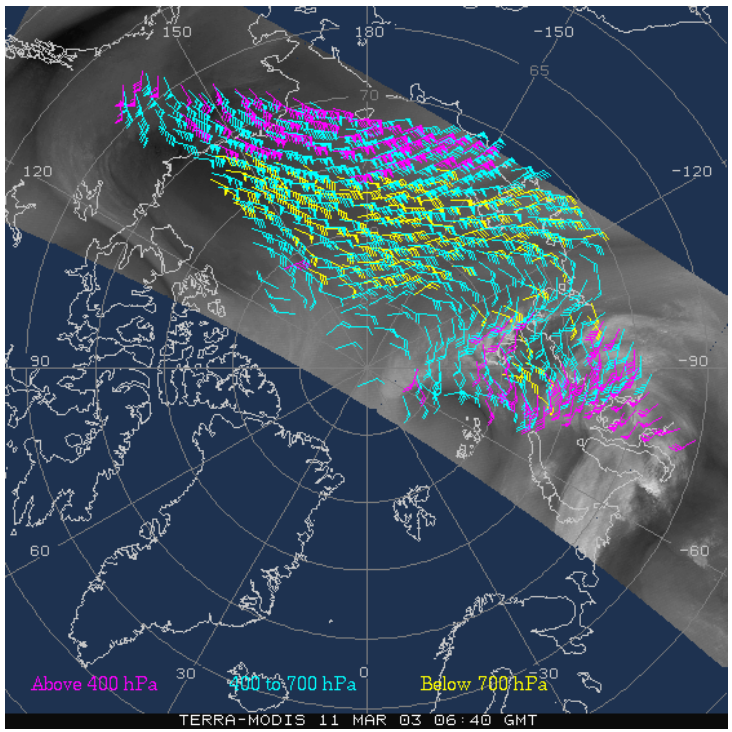

So far, Optical Flow techniques have been used on the observation side, for the purpose of deriving wind vectors by tracking features in IR/WV bands.

[Bormann et al. 2003] have shown that wind vectors have observation errors spatially correlated.

← Figure: AVHRR/MODIS Polar Wind vectors. Product from NOAA/NESDIS.

Let I be a sequence of images on a bounded domain $\Omega \subset \mathcal{R}^2$.
The Optical Flow [Horn and Schunck 1981] is the velocity field $\mathbf{v}$ verifying:

$$I(\mathbf{s} + \mathbf{v}\Delta_t, t + \Delta_t) \approx I(\mathbf{s}, t)$$

Motion estimation is part of most video coding schemes because it enables us to exploit the high degree of temporal redundancy present.

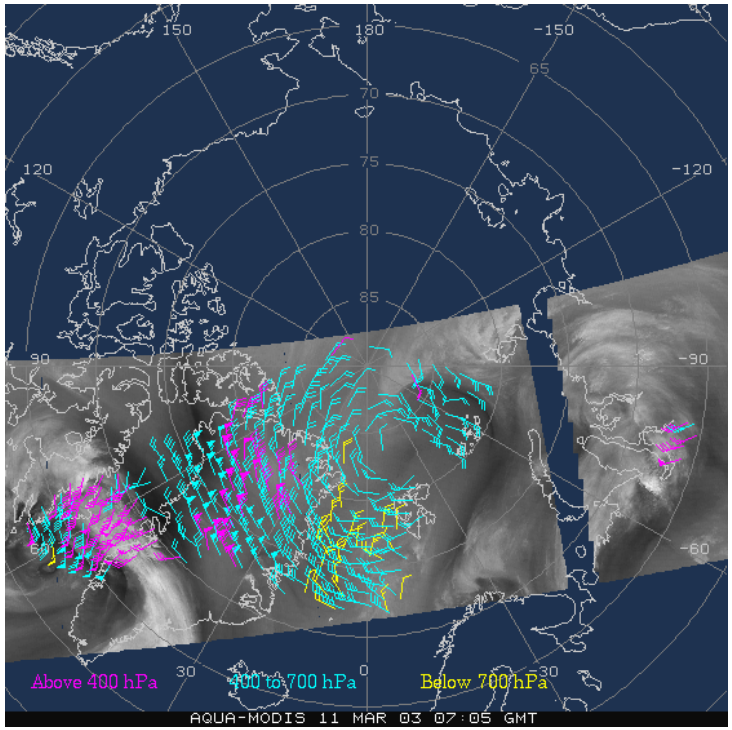

So far, Optical Flow techniques have been used on the observation side, for the purpose of deriving wind vectors by tracking features in IR/WV bands.

[Bormann et al. 2003] have shown that wind vectors have observation errors spatially correlated.

← Figure: AVHRR/MODIS Polar Wind vectors. Product from NOAA/NESDIS.

Let I be a sequence of images on a bounded domain $\Omega \subset \mathcal{R}^2$.
The Optical Flow [Horn and Schunck 1981] is the velocity field $\mathbf{v}$ verifying:

$$I(\mathbf{s} + \mathbf{v}\Delta_t, t + \Delta_t) \approx I(\mathbf{s}, t)$$

Motion estimation is part of most video coding schemes because it enables us to exploit the high degree of temporal redundancy present.

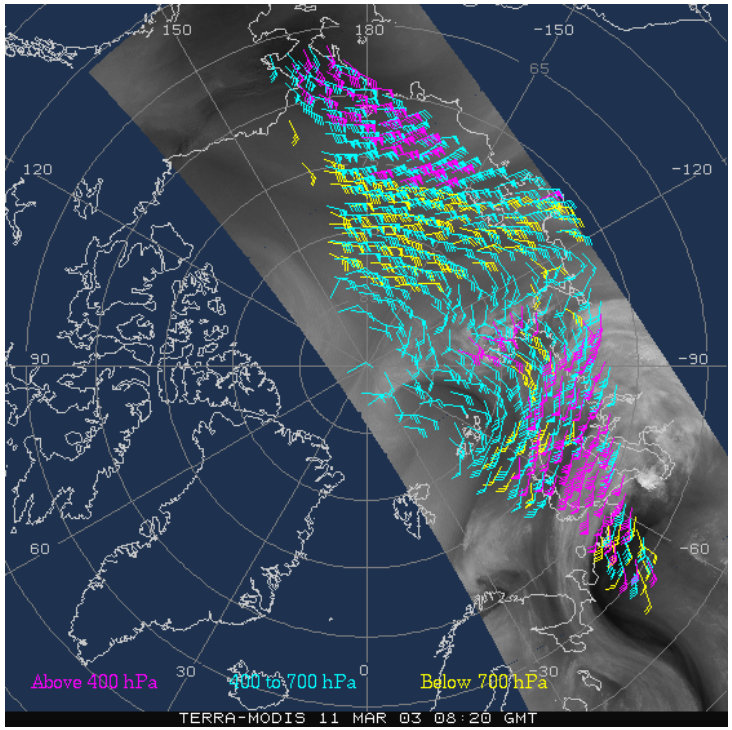

So far, Optical Flow techniques have been used on the observation side, for the purpose of deriving wind vectors by tracking features in IR/WV bands.

[Bormann et al. 2003] have shown that wind vectors have observation errors spatially correlated.

← Figure: AVHRR/MODIS Polar Wind vectors. Product from NOAA/NESDIS.

Let I be a sequence of images on a bounded domain $\Omega \subset \mathcal{R}^2$.
The Optical Flow [Horn and Schunck 1981] is the velocity field $\mathbf{v}$ verifying:

$$I(\mathbf{s} + \mathbf{v}\Delta_t, t + \Delta_t) \approx I(\mathbf{s}, t)$$

Motion estimation is part of most video coding schemes because it enables us to exploit the high degree of temporal redundancy present.

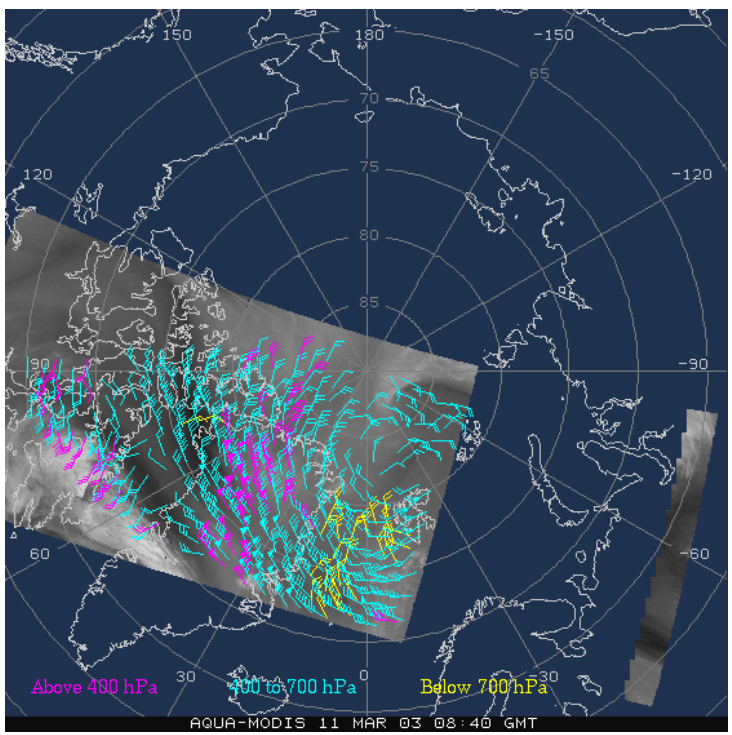

So far, Optical Flow techniques have been used on the observation side, for the purpose of deriving wind vectors by tracking features in IR/WV bands.

[Bormann et al. 2003] have shown that wind vectors have observation errors spatially correlated.

← Figure: AVHRR/MODIS Polar Wind vectors. Product from NOAA/NESDIS.

Let I be a sequence of images on a bounded domain $\Omega \subset \mathcal{R}^2$.
The Optical Flow [Horn and Schunck 1981] is the velocity field $\mathbf{v}$ verifying:

$$I(\mathbf{s} + \mathbf{v}\Delta_t, t + \Delta_t) \approx I(\mathbf{s}, t)$$

Motion estimation is part of most video coding schemes because it enables us to exploit the high degree of temporal redundancy present.

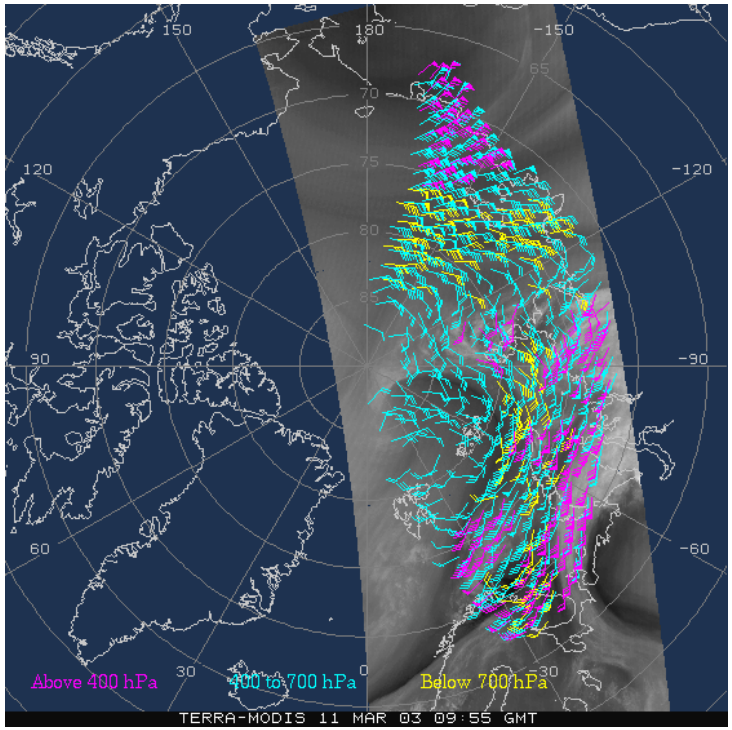

So far, Optical Flow techniques have been used on the observation side, for the purpose of deriving wind vectors by tracking features in IR/WV bands.

[Bormann et al. 2003] have shown that wind vectors have observation errors spatially correlated.

← Figure: AVHRR/MODIS Polar Wind vectors. Product from NOAA/NESDIS.

Let I be a sequence of images on a bounded domain $\Omega \subset \mathcal{R}^2$.
The Optical Flow [Horn and Schunck 1981] is the velocity field $\mathbf{v}$ verifying:

$$I(\mathbf{s} + \mathbf{v}\Delta_t, t + \Delta_t) \approx I(\mathbf{s}, t)$$

Motion estimation is part of most video coding schemes because it enables us to exploit the high degree of temporal redundancy present.

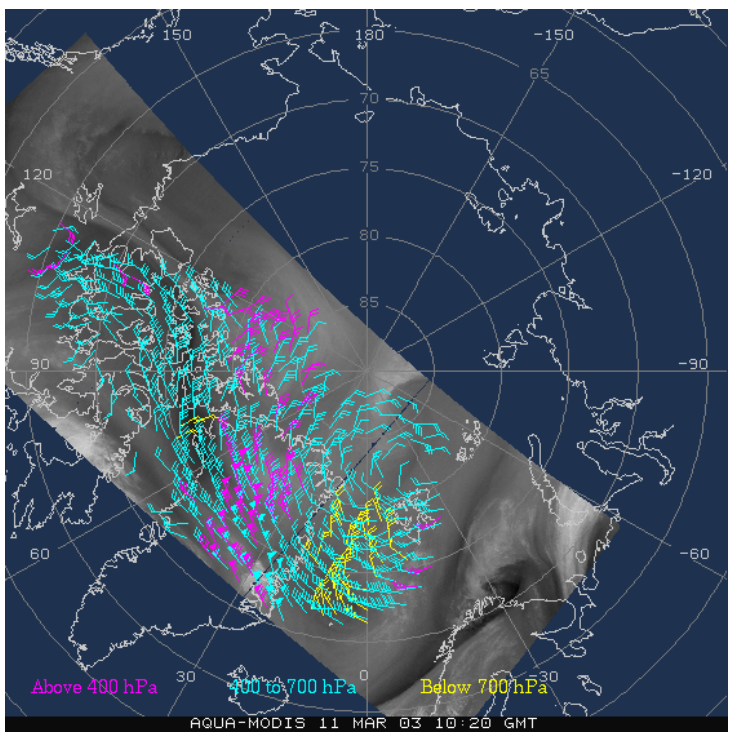

So far, Optical Flow techniques have been used on the observation side, for the purpose of deriving wind vectors by tracking features in IR/WV bands.

[Bormann et al. 2003] have shown that wind vectors have observation errors spatially correlated.

← Figure: AVHRR/MODIS Polar Wind vectors. Product from NOAA/NESDIS.

Let I be a sequence of images on a bounded domain $\Omega \subset \mathcal{R}^2$.
The Optical Flow [Horn and Schunck 1981] is the velocity field $\mathbf{v}$ verifying:

$$I(\mathbf{s} + \mathbf{v}\Delta_t, t + \Delta_t) \approx I(\mathbf{s}, t)$$

Motion estimation is part of most video coding schemes because it enables us to exploit the high degree of temporal redundancy present.

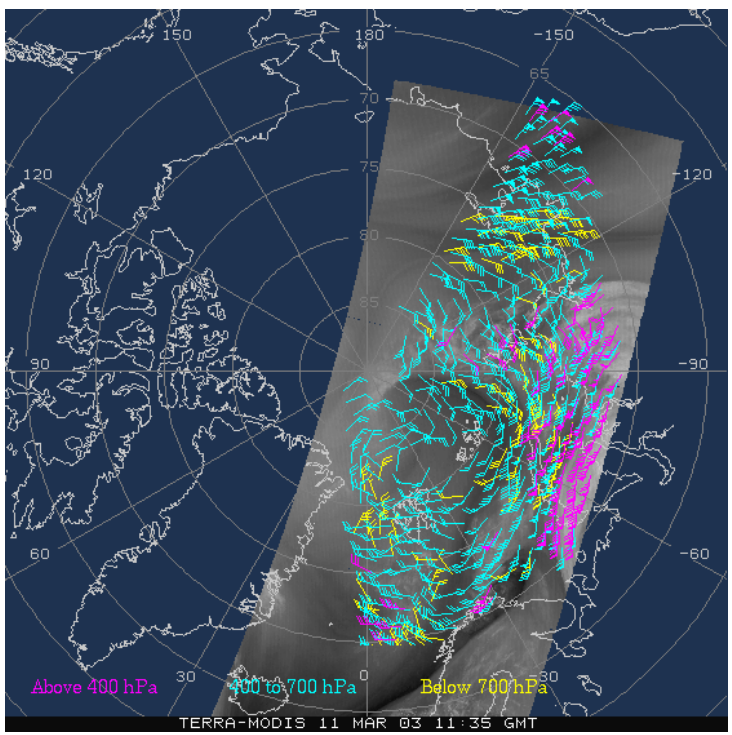

So far, Optical Flow techniques have been used on the observation side, for the purpose of deriving wind vectors by tracking features in IR/WV bands.

[Bormann et al. 2003] have shown that wind vectors have observation errors spatially correlated.

← Figure: AVHRR/MODIS Polar Wind vectors. Product from NOAA/NESDIS.

Let I be a sequence of images on a bounded domain $\Omega \subset \mathcal{R}^2$.
The Optical Flow [Horn and Schunck 1981] is the velocity field $\mathbf{v}$ verifying:

$$I(\mathbf{s} + \mathbf{v}\Delta_t, t + \Delta_t) \approx I(\mathbf{s}, t)$$

Motion estimation is part of most video coding schemes because it enables us to exploit the high degree of temporal redundancy present.

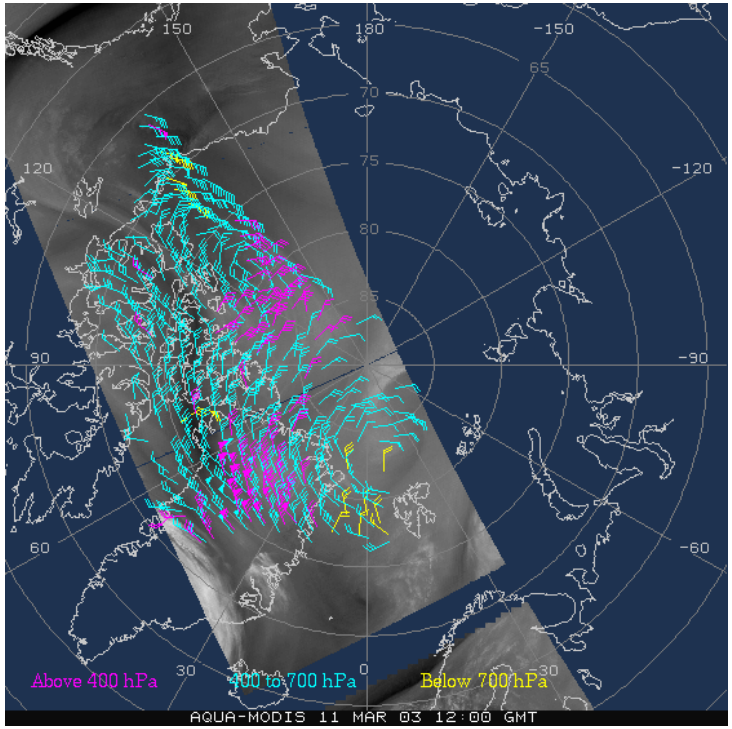

So far, Optical Flow techniques have been used on the observation side, for the purpose of deriving wind vectors by tracking features in IR/WV bands.

[Bormann et al. 2003] have shown that wind vectors have observation errors spatially correlated.

← Figure: AVHRR/MODIS Polar Wind vectors. Product from NOAA/NESDIS.

Let I be a sequence of images on a bounded domain $\Omega \subset \mathcal{R}^2$.
The Optical Flow [Horn and Schunck 1981] is the velocity field $\mathbf{v}$ verifying:

$$I(\mathbf{s} + \mathbf{v}\Delta_t, t + \Delta_t) \approx I(\mathbf{s}, t)$$

Motion estimation is part of most video coding schemes because it enables us to exploit the high degree of temporal redundancy present.

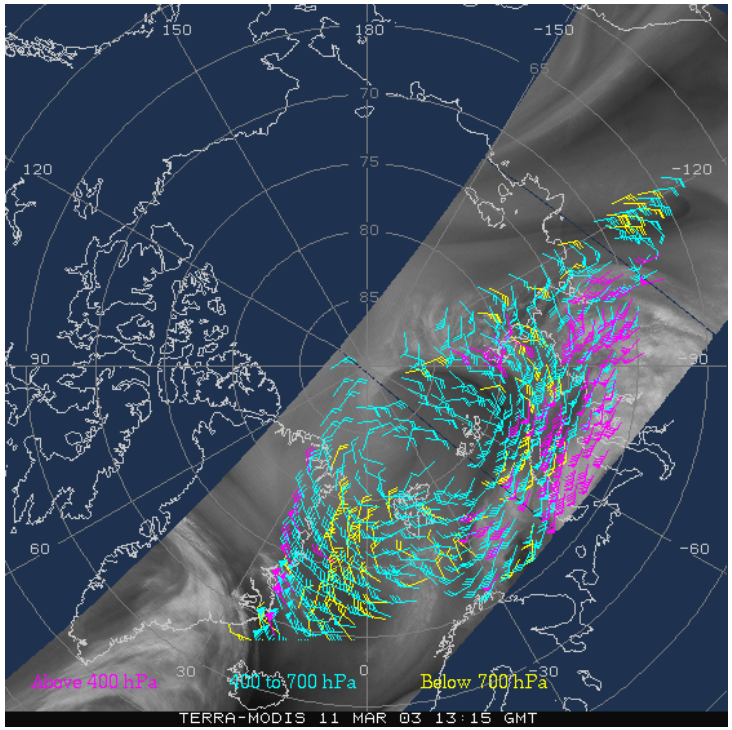

So far, Optical Flow techniques have been used on the observation side, for the purpose of deriving wind vectors by tracking features in IR/WV bands.

[Bormann et al. 2003] have shown that wind vectors have observation errors spatially correlated.

← Figure: AVHRR/MODIS Polar Wind vectors. Product from NOAA/NESDIS.

Let I be a sequence of images on a bounded domain $\Omega \subset \mathcal{R}^2$.
The Optical Flow [Horn and Schunck 1981] is the velocity field $\mathbf{v}$ verifying:

$$I(\mathbf{s} + \mathbf{v}\Delta_t, t + \Delta_t) \approx I(\mathbf{s}, t)$$

Motion estimation is part of most video coding schemes because it enables us to exploit the high degree of temporal redundancy present.

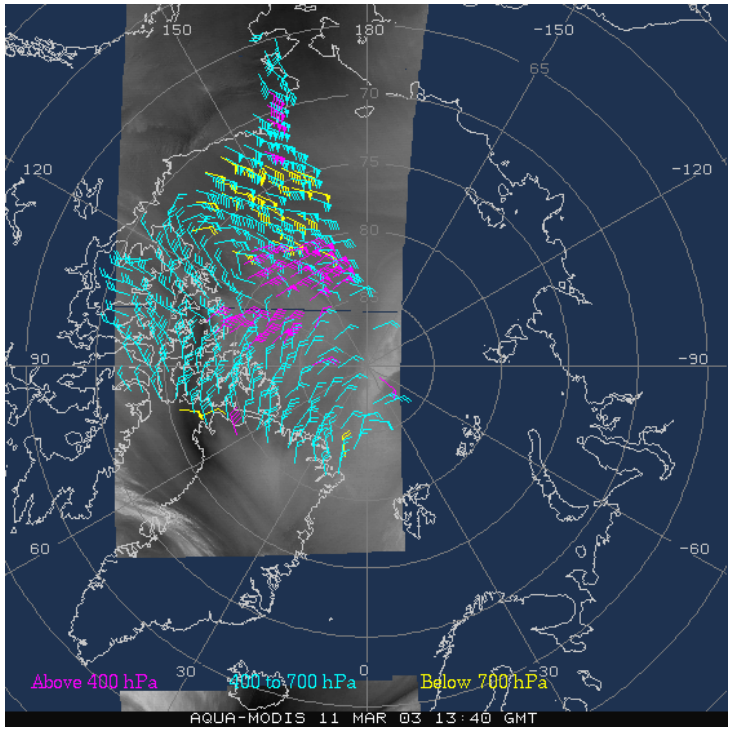

So far, Optical Flow techniques have been used on the observation side, for the purpose of deriving wind vectors by tracking features in IR/WV bands.

[Bormann et al. 2003] have shown that wind vectors have observation errors spatially correlated.

← Figure: AVHRR/MODIS Polar Wind vectors. Product from NOAA/NESDIS.

Let I be a sequence of images on a bounded domain $\Omega \subset \mathcal{R}^2$.
The Optical Flow [Horn and Schunck 1981] is the velocity field $\mathbf{v}$ verifying:

$$I(\mathbf{s} + \mathbf{v}\Delta_t, t + \Delta_t) \approx I(\mathbf{s}, t)$$

Motion estimation is part of most video coding schemes because it enables us to exploit the high degree of temporal redundancy present.

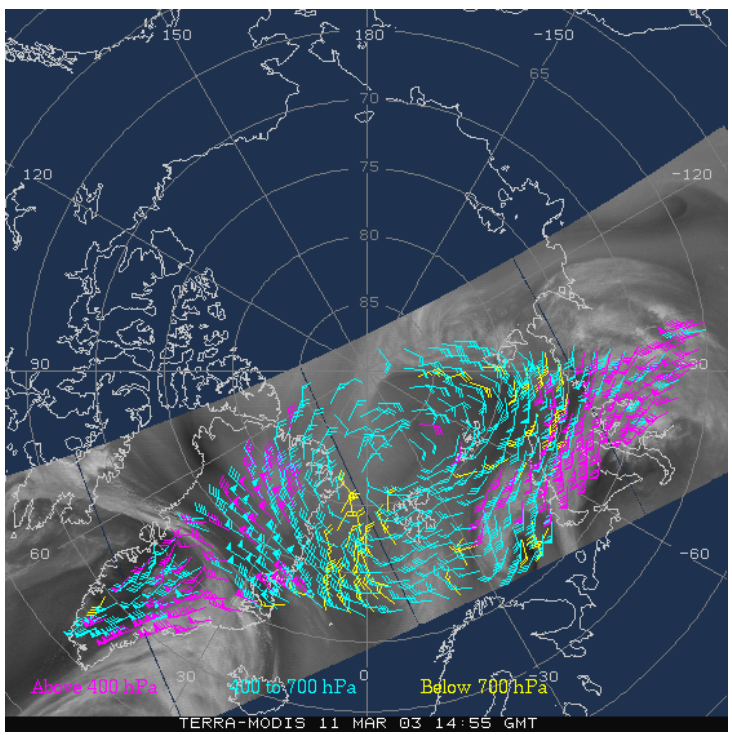

So far, Optical Flow techniques have been used on the observation side, for the purpose of deriving wind vectors by tracking features in IR/WV bands.

[Bormann et al. 2003] have shown that wind vectors have observation errors spatially correlated.

← Figure: AVHRR/MODIS Polar Wind vectors. Product from NOAA/NESDIS.

Let I be a sequence of images on a bounded domain $\Omega \subset \mathcal{R}^2$.
The Optical Flow [Horn and Schunck 1981] is the velocity field $\mathbf{v}$ verifying:

$$I(\mathbf{s} + \mathbf{v}\Delta_t, t + \Delta_t) \approx I(\mathbf{s}, t)$$

Motion estimation is part of most video coding schemes because it enables us to exploit the high degree of temporal redundancy present.

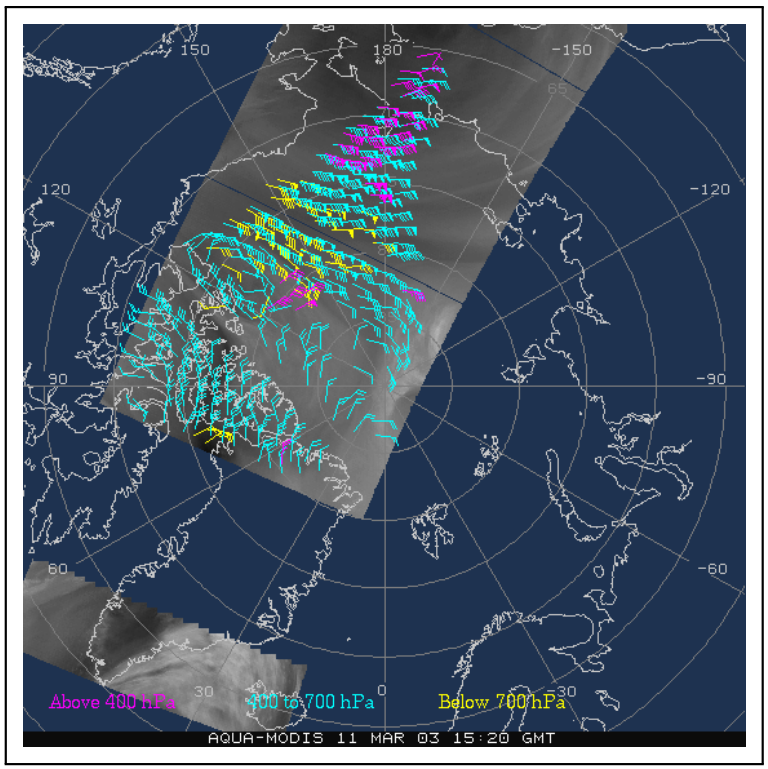

So far, Optical Flow techniques have been used on the observation side, for the purpose of deriving wind vectors by tracking features in IR/WV bands.

[Bormann et al. 2003] have shown that wind vectors have observation errors spatially correlated.

← Figure: AVHRR/MODIS Polar Wind vectors. Product from NOAA/NESDIS.

Let I be a sequence of images on a bounded domain $\Omega \subset \mathcal{R}^2$.
The Optical Flow [Horn and Schunck 1981] is the velocity field $\mathbf{v}$ verifying:

$$I(\mathbf{s} + \mathbf{v}\Delta_t, t + \Delta_t) \approx I(\mathbf{s}, t)$$

Motion estimation is part of most video coding schemes because it enables us to exploit the high degree of temporal redundancy present.

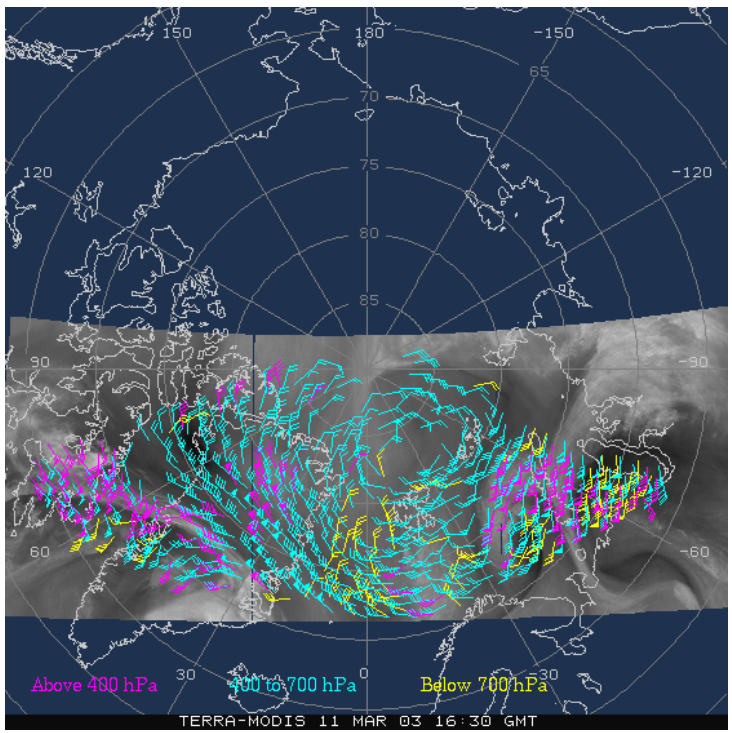

So far, Optical Flow techniques have been used on the observation side, for the purpose of deriving wind vectors by tracking features in IR/WV bands.

[Bormann et al. 2003] have shown that wind vectors have observation errors spatially correlated.

← Figure: AVHRR/MODIS Polar Wind vectors. Product from NOAA/NESDIS.

Let I be a sequence of images on a bounded domain $\Omega \subset \mathcal{R}^2$.
The Optical Flow [Horn and Schunck 1981] is the velocity field $\mathbf{v}$ verifying:

$$I(\mathbf{s} + \mathbf{v}\Delta_t, t + \Delta_t) \approx I(\mathbf{s}, t)$$

Motion estimation is part of most video coding schemes because it enables us to exploit the high degree of temporal redundancy present.

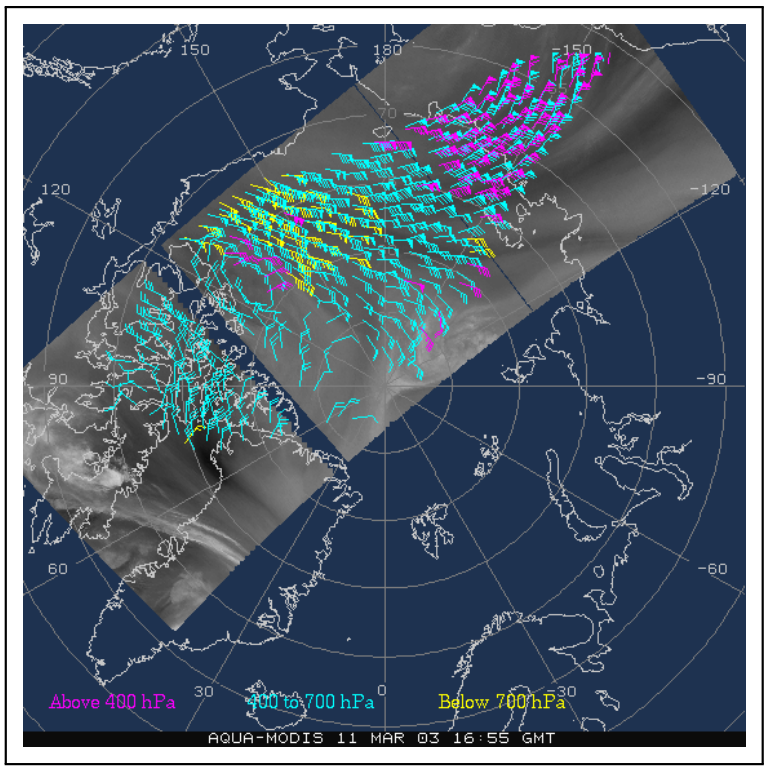

So far, Optical Flow techniques have been used on the observation side, for the purpose of deriving wind vectors by tracking features in IR/WV bands.

[Bormann et al. 2003] have shown that wind vectors have observation errors spatially correlated.

← Figure: AVHRR/MODIS Polar Wind vectors. Product from NOAA/NESDIS.

Let I be a sequence of images on a bounded domain $\Omega \subset \mathcal{R}^2$.
The Optical Flow [Horn and Schunck 1981] is the velocity field $\mathbf{v}$ verifying:

$$I(\mathbf{s} + \mathbf{v}\Delta_t, t + \Delta_t) \approx I(\mathbf{s}, t)$$

Motion estimation is part of most video coding schemes because it enables us to exploit the high degree of temporal redundancy present.

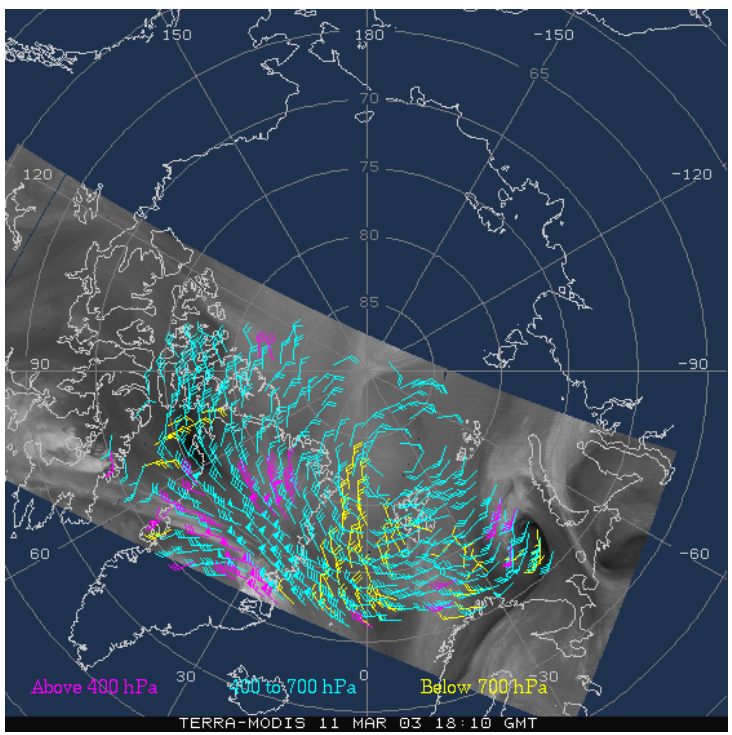

So far, Optical Flow techniques have been used on the observation side, for the purpose of deriving wind vectors by tracking features in IR/WV bands.

[Bormann et al. 2003] have shown that wind vectors have observation errors spatially correlated.

← Figure: AVHRR/MODIS Polar Wind vectors. Product from NOAA/NESDIS.

Let I be a sequence of images on a bounded domain $\Omega \subset \mathcal{R}^2$.
The Optical Flow [Horn and Schunck 1981] is the velocity field $\mathbf{v}$ verifying:

$$I(\mathbf{s} + \mathbf{v}\Delta_t, t + \Delta_t) \approx I(\mathbf{s}, t)$$

Motion estimation is part of most video coding schemes because it enables us to exploit the high degree of temporal redundancy present.

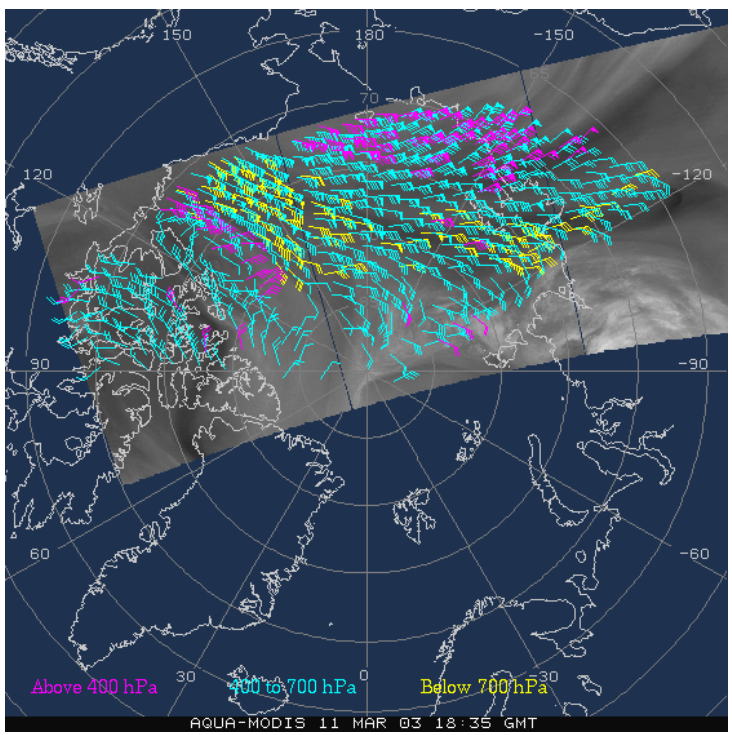

So far, Optical Flow techniques have been used on the observation side, for the purpose of deriving wind vectors by tracking features in IR/WV bands.

[Bormann et al. 2003] have shown that wind vectors have observation errors spatially correlated.

← Figure: AVHRR/MODIS Polar Wind vectors. Product from NOAA/NESDIS.

Let I be a sequence of images on a bounded domain $\Omega \subset \mathcal{R}^2$.
The Optical Flow [Horn and Schunck 1981] is the velocity field $\mathbf{v}$ verifying:

$$I(\mathbf{s} + \mathbf{v}\Delta_t, t + \Delta_t) \approx I(\mathbf{s}, t)$$

Motion estimation is part of most video coding schemes because it enables us to exploit the high degree of temporal redundancy present.

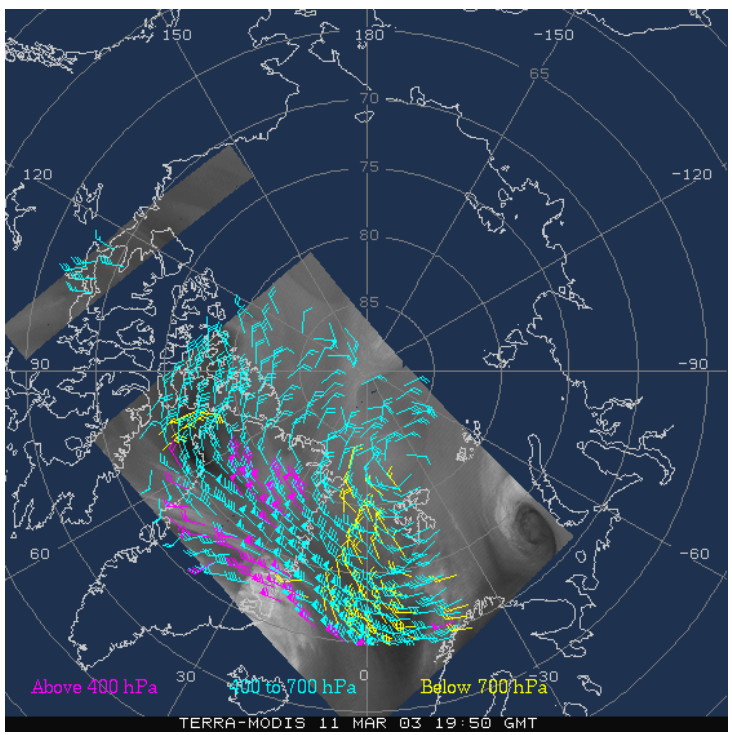

So far, Optical Flow techniques have been used on the observation side, for the purpose of deriving wind vectors by tracking features in IR/WV bands.

[Bormann et al. 2003] have shown that wind vectors have observation errors spatially correlated.

← Figure: AVHRR/MODIS Polar Wind vectors. Product from NOAA/NESDIS.

Let I be a sequence of images on a bounded domain $\Omega \subset \mathcal{R}^2$.
The Optical Flow [Horn and Schunck 1981] is the velocity field $\mathbf{v}$ verifying:

$$I(\mathbf{s} + \mathbf{v}\Delta_t, t + \Delta_t) \approx I(\mathbf{s}, t)$$

Motion estimation is part of most video coding schemes because it enables us to exploit the high degree of temporal redundancy present.

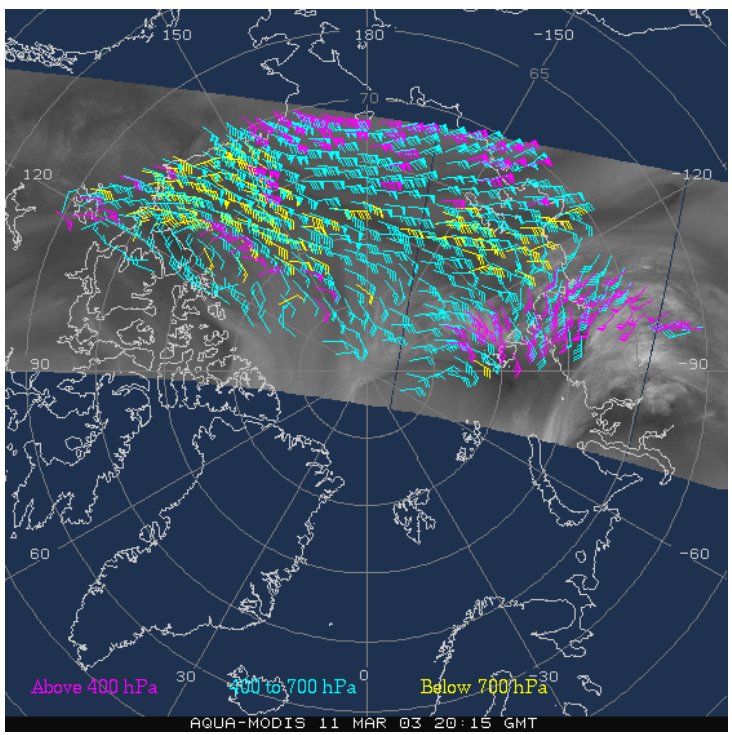

So far, Optical Flow techniques have been used on the observation side, for the purpose of deriving wind vectors by tracking features in IR/WV bands.

[Bormann et al. 2003] have shown that wind vectors have observation errors spatially correlated.

← Figure: AVHRR/MODIS Polar Wind vectors. Product from NOAA/NESDIS.

Let I be a sequence of images on a bounded domain $\Omega \subset \mathcal{R}^2$.
The "Optical Flow" is the velocity field $\mathbf{v}$ verifying:

$$\mathbf{v} = \text{Argmin}\left\{||I(\mathbf{s} + \mathbf{v}\Delta_t, t + \Delta_t) - I(\mathbf{s}, t)||^2 + \mathcal{L}(\mathbf{v})\right\}$$

Motion estimation is part of most video coding schemes because it enables us to exploit the high degree of temporal redundancy present.

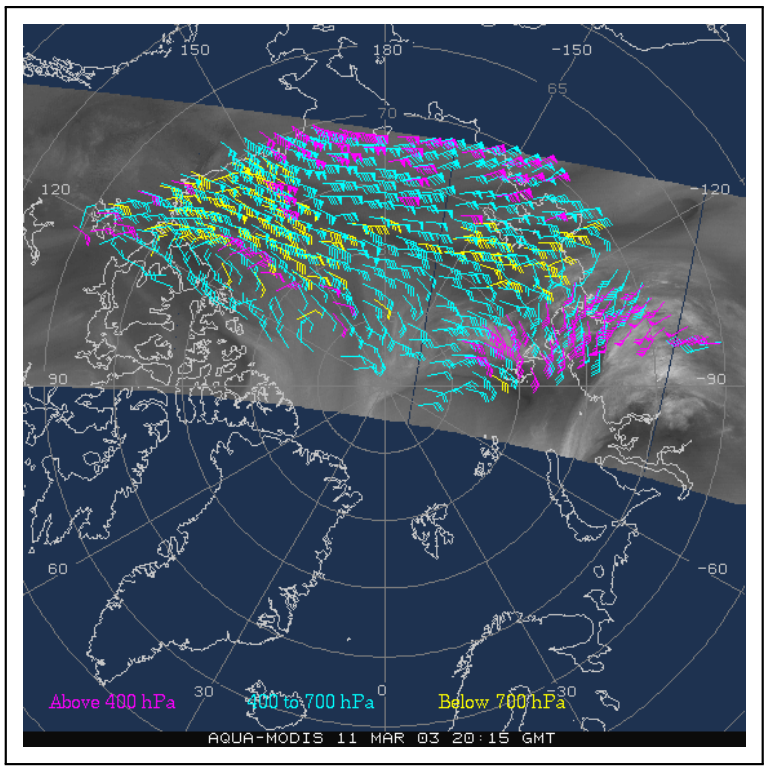

So far, Optical Flow techniques have been used on the observation side, for the purpose of deriving wind vectors by tracking features in IR/WV bands.

[Bormann et al. 2003] have shown that wind vectors have observation errors spatially correlated.

← Figure: AVHRR/MODIS Polar Wind vectors. Product from NOAA/NESDIS.

Data assimilation

Data assimilation seeks for the state $\boldsymbol{x}$ that is most probable given a set of observations $\boldsymbol{y}$ and an *a-priori* background information $\boldsymbol{x}_b$.

$$\mathbb{P}(\boldsymbol{x}|\boldsymbol{y}) \propto \mathbb{P}(\boldsymbol{y}|\boldsymbol{x})\mathbb{P}(\boldsymbol{x})$$

Under the Gaussian assumption:

$$\mathbb{P}(\boldsymbol{x}) \propto e^{-\frac{1}{2}(\boldsymbol{x}-\boldsymbol{x_b})^{\mathrm{T}} B^{-1}(\boldsymbol{x}-\boldsymbol{x_b})}$$

$$\mathbb{P}(\boldsymbol{y}|\boldsymbol{x}) \propto e^{-\frac{1}{2}(\boldsymbol{y}-\mathcal{H}\boldsymbol{x})^{\mathrm{T}} R^{-1}(\boldsymbol{y}-\mathcal{H}\boldsymbol{x})}$$

Variational formulation: the analysis $\boldsymbol{x}_a$ may be seen as realizing the minimum of a cost function $\mathcal{J}$:

$$\begin{aligned}
\boldsymbol{x}_a &= \text{Argmin } \mathcal{J} \\
\mathcal{J}(\boldsymbol{x}) &= J_b(\boldsymbol{x}) + J_o(\boldsymbol{x}) \\
\mathcal{J}(\boldsymbol{x}) &= \underbrace{\frac{1}{2}(\boldsymbol{x}-\boldsymbol{x}_b)^{\mathrm{T}} B^{-1}(\boldsymbol{x}-\boldsymbol{x}_b)}_{\text{background departure}} + \underbrace{\frac{1}{2}\sum_{i=0}^{n}\left(\boldsymbol{y_i}-\mathcal{H}_i(\boldsymbol{x_i})\right)^{\mathrm{T}} {R_i}^{-1}\left(\boldsymbol{y_i}-\mathcal{H}_i(\boldsymbol{x_i})\right)}_{\text{observations departure}}
\end{aligned}$$

Observations $\boldsymbol{y}$ of hurricane position can be assimilated with an EnKF given an observation operator that computes the position of the vortex $\sim \mathrm{Max}_{\Omega}(\zeta)$. The linear updating scheme used in the EnKF is effective for small displacements [Chen and Snyder 2007].

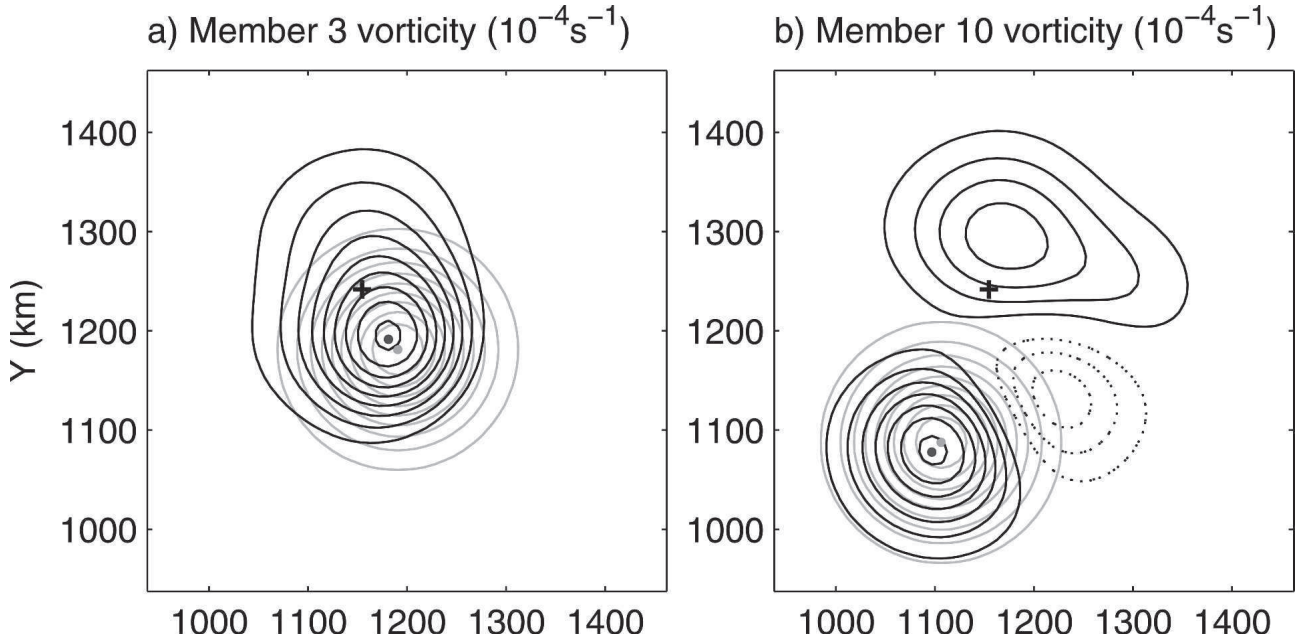

FIG. 2. Prior (gray contours) and posterior (black contours) vorticities of members (a) 3 and (b) 10 for initial position errors of σ_f = 80 km. The contours have intervals of 0.5 × 10^{-4} s^{-1} with zero contours omitted and negative values dotted. The gray dot, the black dot, and the cross denote the prior, posterior, and observed centers, respectively.

Figure: EnKF analysis updates for a vortex position observation with (a) small (b) large displacement error [Chen and Snyder 2007].

$$\mathbb{P}(\boldsymbol{x}, \boldsymbol{q}|\boldsymbol{y}) \propto \mathbb{P}(\boldsymbol{y}|\boldsymbol{x}, \boldsymbol{q})\mathbb{P}(\boldsymbol{x})\mathbb{P}(\boldsymbol{q})$$

The Morphing Ensemble Kalman Filter

$$J(T, u, v) = \|v - u \circ (I + T)\| + C_1\|T\| + C_2\| \bigtriangledown T\| \to \min_T,$$

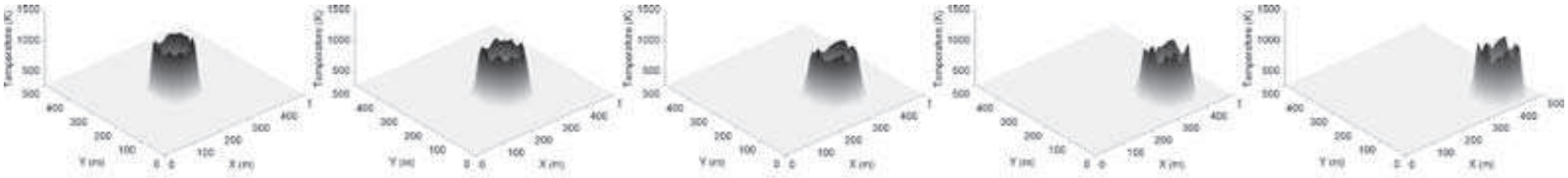

Fig. 2. Morphing of two solutions of a reaction-diffusion equation system used in a wildfire simulation. The states with $\lambda = 0$ and $\lambda = 1$ are given. The intermediate states are created automatically. The horizontal plane is the earth surface. The vertical axis and the colour map are the temperature. The morphing algorithm combines the values as well as the positions.

Figure: From [Beezley and Mandel 2008].

The Field Alignment Data Assimilation

$$\begin{aligned} J_2(X, \mathbf{q}) = & \frac{1}{2}(X(\mathbf{p}) - X^f(\mathbf{p}))^{\mathrm{T}} B(\mathbf{q})^{-1}(X(\mathbf{p}) - X^f(\mathbf{p})) \\ & + \frac{1}{2}(Y - H\ X(\mathbf{p}))^{\mathrm{T}} R^{-1}(Y - H\ X(\mathbf{p})) \\ & + L(\mathbf{q}) - \frac{1}{2}\ln(|B(\mathbf{q})|) \end{aligned} \tag{14}$$

$$L(\mathbf{q}) = \frac{w_1}{2}\sum_{j\in\Omega} \mathbf{tr}\{[\nabla \underline{q}_j][\nabla \underline{q}_j]^{\mathrm{T}}\} + \frac{w_2}{2}\sum_{j\in\Omega}[\nabla \cdot \underline{q}_j]^2 \tag{13}$$

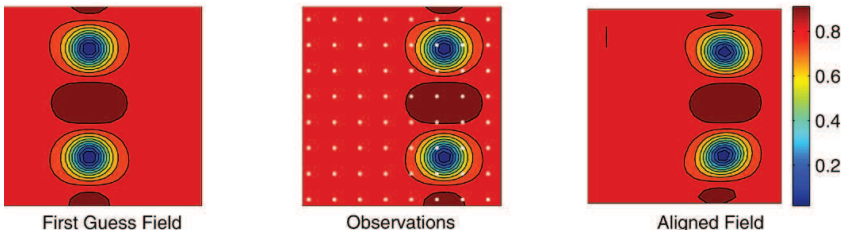

Figure: A two vortex example. From [Ravela et al. 2007].

Tropopause height observations $\boldsymbol{y}_d$ are derived from WV imagery [Michel and Bouttier 2006, Michel 2009] by regression with WV brightness temperature:

$$P^o_{\text{Tropopause}} = \Gamma\, T_{\text{BB}} + \Lambda$$

Standard amplitude error modelling

$$\boldsymbol{x}_a = \boldsymbol{x}_b + \boldsymbol{\delta x}_a$$
$$\boldsymbol{\delta x}_a = BH^{\mathrm{T}}(HBH^{\mathrm{T}} + R)^{-1}(\boldsymbol{y} - H\boldsymbol{x}_b)$$

B is the background error covariance matrix.
Our pseudo-observations write:

$$\boldsymbol{y} = 1.5 \text{ PVU}$$
$$\text{at } P = P^o_{\text{Tropopause}}$$

Standard deviation of "linearized" error:
$\sigma_o^{PV} = \text{Stdev}(P^o_{\text{Tropopause}} - \Gamma\, T_{\text{BB}} - \Lambda) \times \frac{\partial \mathcal{H}_{\text{PV}}}{\partial p}\big|_{p=P^o_{\text{Tropopause}}}$

Tropopause height observations $\boldsymbol{y}_d$ are derived from WV imagery [Michel and Bouttier 2006, Michel 2009] by regression with WV brightness temperature:

$$P^o_{\text{Tropopause}} = \Gamma\, T_{\text{BB}} + \Lambda$$

Alternative alignment error modeling [Lawson and Hansen 2005]

$$\boldsymbol{x}_a = \boldsymbol{x}_b\big(\boldsymbol{s} + \boldsymbol{\delta s}_a\big)$$
$$\boldsymbol{\delta s}_a = DH_d^{\mathrm{T}}(H_d D H_d^{\mathrm{T}} + R_d)^{-1}(\boldsymbol{y}_d - H_d \boldsymbol{x}_b)$$

D is the alignment background error covariance matrix.
Our pseudo-observations write:

$$\boldsymbol{y_d} = P^o_{\text{Tropopause}}$$
$$\text{at } PV = 1.5 \text{ PVU}$$

Standard deviation:
$\sigma_{od}^{PV} = \text{Stdev}(P^o_{\text{Tropopause}} - \Gamma\, T_{\text{BB}} - \Lambda)$

B

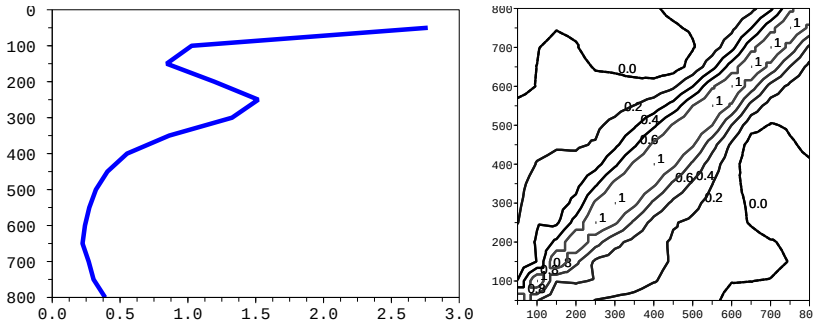

(a) σ_b (b) Correlations

D

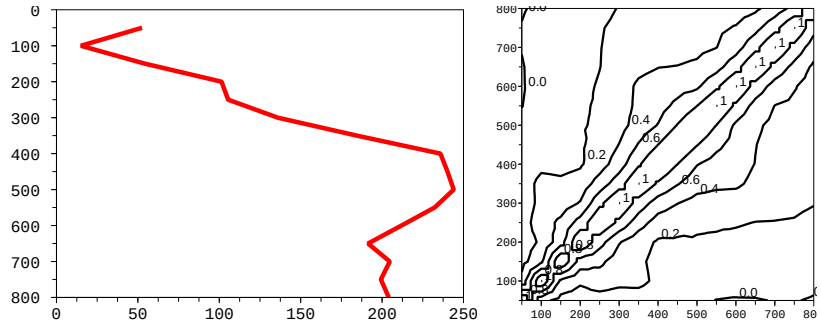

(a) σ_d (b) Correlations

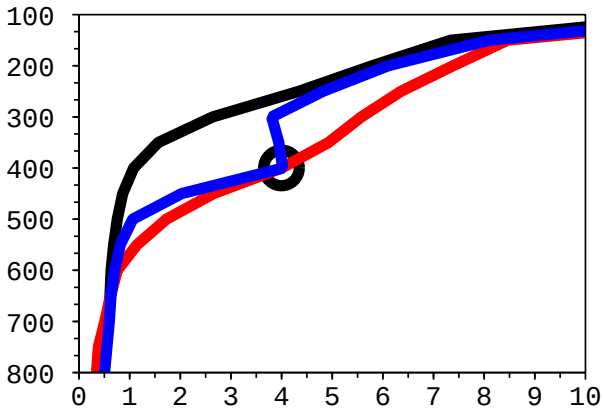

Single observation experiment [Michel 2009]
Strong differences may exist between the shape of the two analysis (amplitude and alignment)

Use of unconstrained displacement to calibrate a J_d (*e.g.* a covariance model for displacement errors) has also been investigated by [Nehrkorn et al. 2003] with the "feature calibration and alignment" method.

Some Questions in the Amplitude-Position Data Assimilation

Standard DA may not be able to correct coherent structures in the flow. Alignment/Amplitude-Position DA extends the control variable to include some displacement field, and is considered as a big step beyond bogussing techniques or use of linearized operators.

ACAPS

Amplitude-Position Data Assimilation is considered as a candidate for the integrated AFWA Coupled Analysis and Prediction System (ACAPS). This system will require state-of-the-art cloud analysis capabilities [Auligné 2010]

Questions

- Bayesian interpretation of Tikhonov regularization
- Does displacement preserve balance?
- How may we separate displacement from amplitude errors?
- Non-linearity of Optimization (shared with Optical Flow problem)

Outline

Outline

Bayesian Interpretation of Tikhonov Regularizations

Data Assimilation Bayesian Framework	Optical Flow Regularization
Constraints come from knowledge on background error statistics (*e.g.* sample **B** in EnKF balance + calibrated covariance operators in 3D/4D-Var).	Constraints are formulated as Tikhonov regularization that requires local smoothness of the field.

May we link the two options?

Bayesian Interpretation of Tikhonov Regularizations

Data Assimilation Bayesian Framework	Optical Flow Regularization
Constraints come from knowledge on background error statistics (*e.g.* sample $\mathbf{B}$ in EnKF balance + calibrated covariance operators in 3D/4D-Var).	Constraints are formulated as Tikhonov regularization that requires local smoothness of the field.

May we link the two options? - Yes!
[Oliver 1998, Tarantola 2005, Bérézia t and Herlin 2010].

Inverse $\mathbf{D^{-1}}$ of a covariance matrix $\mathbf{D}$ is formally

$$\int \mathbf{D^{-1}}(\mathbf{x},\mathbf{x''})\mathbf{D}(\mathbf{x''},\mathbf{x'})d\mathbf{x''} = \delta_{\text{DIRAC}}(\mathbf{x}-\mathbf{x'}) \tag{1}$$

In the simpler case where $\mathbf{D}$ is stationary $\mathbf{D}(\mathbf{x},\mathbf{x'}) = c(\mathbf{x}-\mathbf{x'})$:

$$c^{-1} \star c(\mathbf{x}) = \delta_{\text{DIRAC}}(\mathbf{x}) \tag{2}$$

$$\widehat{c^{-1}}(\omega) = \frac{1}{\widehat{c(\omega)}} \tag{3}$$

There are a few examples where inverse covariance may be found analytically.

Inverse of Exponential Covariance

For instance, exponential model is defined by $c(\mathbf{x}) = \exp\left(-\frac{|\mathbf{x}|}{L}\right)$.

Fourier transform is $\widehat{c}(\omega) = \frac{2L}{1+L^2\omega^2}$.

$$\widehat{c^{-1}}(\omega) = \frac{1+L^2\omega^2}{2L}, \text{ such that } c^{-1}(\mathbf{x}) = \frac{1}{2L}\left(\delta_{\text{DIRAC}}(\mathbf{x}) - L^2\delta''_{\text{DIRAC}}(\mathbf{x})\right)$$

Replacing this formal expression into the functional yields:

$$\iint F(\mathbf{X})^{\mathrm{T}}(\mathbf{x})\mathbf{D^{-1}}(\mathbf{x},\mathbf{x}')F(\mathbf{X})(\mathbf{x}')d\mathbf{x}d\mathbf{x}'$$

$$= \frac{1}{2L}\int F(\mathbf{X})^{\mathrm{T}}(\mathbf{x})\left(F(\mathbf{X}) - L^2\frac{\partial^2 F(\mathbf{X}}{\partial \mathbf{x}^2}\right)d\mathbf{x}$$

$$= \frac{1}{2L}\int \left(||F(\mathbf{X})||^2 + L^2||\frac{\partial F(\mathbf{X}}{\partial \mathbf{x}}||^2\right)d\mathbf{x}$$

Exponential covariance is associated to first-order regularization.

A framework for position assimilation has been developed to study equivalence between Tikhonov Regularizations and Covariance Models. A "Single Observation Displacement" $\mathbf{s}_0 = [1, 1]^{\mathrm{T}}$ is assimilated by minimizing the cost function:

$$J(\mathbf{s}) = J_o(\mathbf{s}) + J_d(\mathbf{s}) = ||\mathbf{s} - \mathbf{s}_0||^2 + \mathcal{L}(\mathbf{s})$$

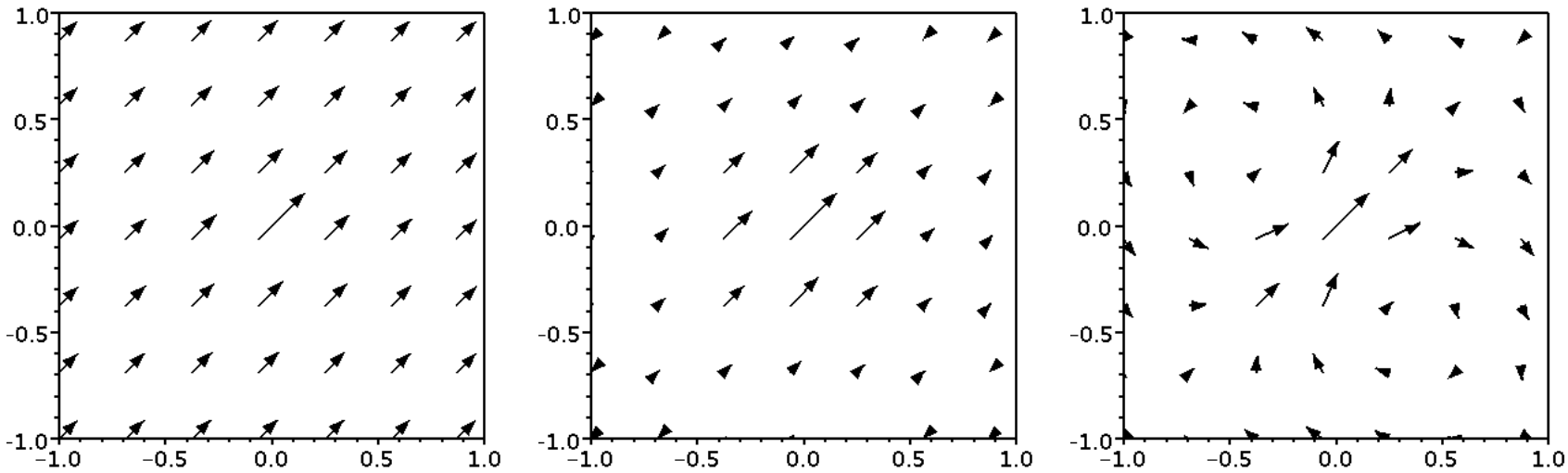

(a) $J_d = w_1||\mathbf{s}||^2 + w_2||\nabla\mathbf{s}||^2$ (b) $J_d = w_1||\mathbf{s}||^2 + w_2||\Delta\mathbf{s}||^2$ (c) $J_d = w_1||\mathbf{s}||^2 + w_2||\nabla\cdot\mathbf{s}||^2$

This shows how Tikhonov Regularizations $\mathcal{L}$ are equivalent to covariance models J_d. ACAPS could take profit of WRF-Var wind analysis routines to build objective/calibrated J_d.

Linearized version of Optical Flow is minimizing

$$||I(\mathbf{s}, t+\Delta_t) - I(\mathbf{s}, t) + \mathbf{v}\Delta_t \nabla I(\mathbf{s}, t+\Delta_t)||^2 + \mathcal{L}(\mathbf{v})$$

instead of

$$||I(\mathbf{s}+\mathbf{v}\Delta_t, t+\Delta_t) - I(\mathbf{s}, t)||^2 + \mathcal{L}(\mathbf{v})$$

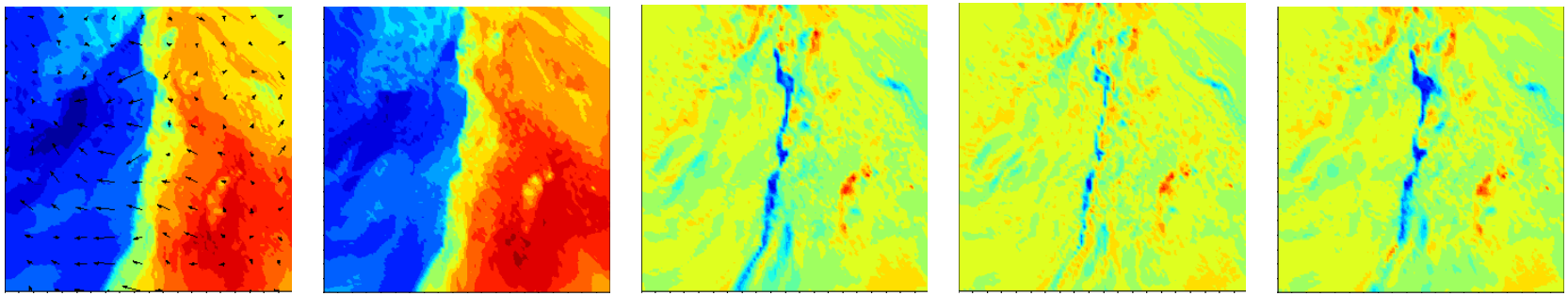

(a) I_1 (b) I_2 (c) Residual (d) L. Residual (e) NL. Residual

Figure: Dowell and Stensrud (2008) dataset of convective scale EnKF. Specific Humidity fields at the surface

Need to consider more advanced multi-scale minimization schemes [Beezley and Mandel 2008, Yang and Ravela 2009].

Conclusion

Amplitude-Position Data Assimilation

Amplitude-Position Data Assimilation tries to distort the background to fit the observations. It may be a solution to assimilate coherent structures related observations (tropical cyclones, clouds, water vapor and PV...).

Tikhonov Regularization

Most studies assume that displacement is locally regular, and incorporate smoothness penalty terms.
Tikhonov Regularizations are equivalent to inverse covariance operators.
Therefore, it may be better to use covariance modeling, as it can be objectively calibrated (for instance by using unconstrained displacement fields to build a "J_d").
Tools to study this problem have been developed during my stay @NCAR.

Minimization

Need to develop efficient advanced minimization schemes.

Outline

Spectral Diagonal Modeling [Berre 2000] is used in operational AROME DA. Very convenient (Inverse, Wiener Khinchin) but limited to stationarity. Wavelet is "natural" extension [Deckmyn and Berre 2005].

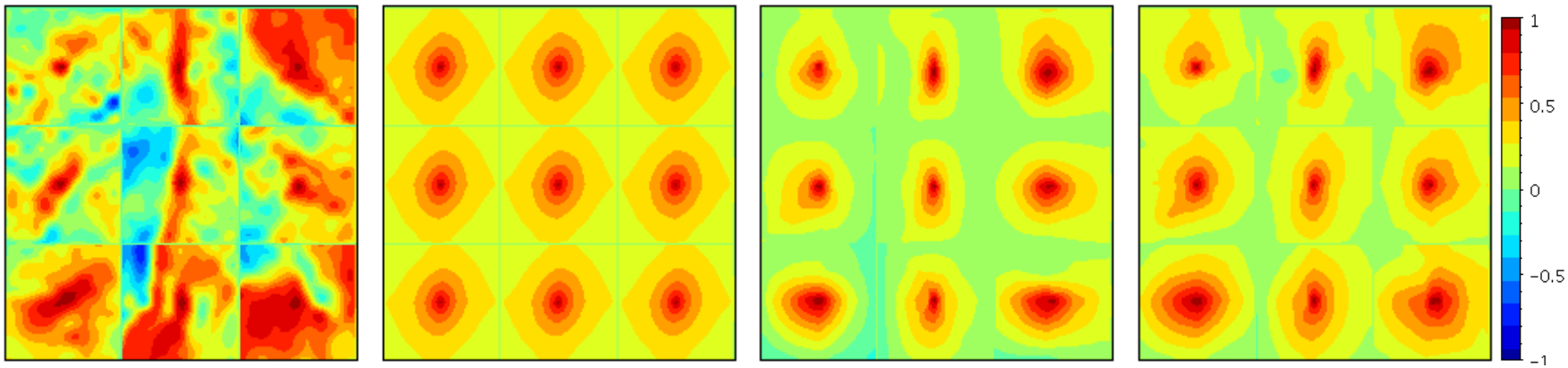

(a) Sample (b) $\mathbf{F}^{-1}\mathbf{D_f}\mathbf{D_f}^{\mathrm{T}}\mathbf{F}$ (c) $\mathbf{W}^{-1}\mathbf{D_w}\mathbf{D_w}^{\mathrm{T}}\mathbf{W}$ (d) Hybrid

Figure: Spectral $\mathbf{F}$ Wavelet $\mathbf{W}$ and Hybrid diagonal correlation modeling on the [Dowell and Stensrud 2008] dataset, for variable q_u at surface.

- Non-dyadic, orthogonal, boundary corrected wavelet transform is under study for $\mathbf{B}$ in WRF-Var [Fournier 2010]
- Q-shift Dual-Tree Complex wavelet transform [Kingsbury 2001] is under study for $\mathbf{B}$ in AROME [Deckmyn 2010].

First-Order Homogeneous Recursive Filtering is used in operational WRF-Var. Convenient because it can easily handle boundaries (ocean DA).

- High-Order (In)homogeneous Recursive Filtering has been developed for use in WRF-Var [Michel and Auligné 2010]
- Anisotropic version is being developed at NCEP [Purser et al. 2003]

Requires local lengthscales as an input [Wu et al. 2002].
Following [BeloPereira and Berre 2006], the inertia matrix of correlation function is

$$\mathbf{N} = \begin{pmatrix} 1/\mathcal{N}_{xx} & 1/\mathcal{N}_{xy} \\ 1/\mathcal{N}_{xy} & 1/\mathcal{N}_{yy} \end{pmatrix} \text{ where } \mathcal{N}_{xy} = \frac{\sigma^2(\epsilon)}{\left\langle \frac{\partial \epsilon}{\partial x} \frac{\partial \epsilon}{\partial y} \right\rangle - \frac{\partial \sigma(\epsilon)}{\partial x} \frac{\partial \sigma(\epsilon)}{\partial y}}$$

Local correlation function:

$$c(\mathbf{s}) \propto e^{-\frac{1}{2}(\mathbf{s}^T \mathbf{N} \mathbf{s})}$$

Better results with spatial filtering of $\mathbf{N}$. May be used for localization in EnKF.

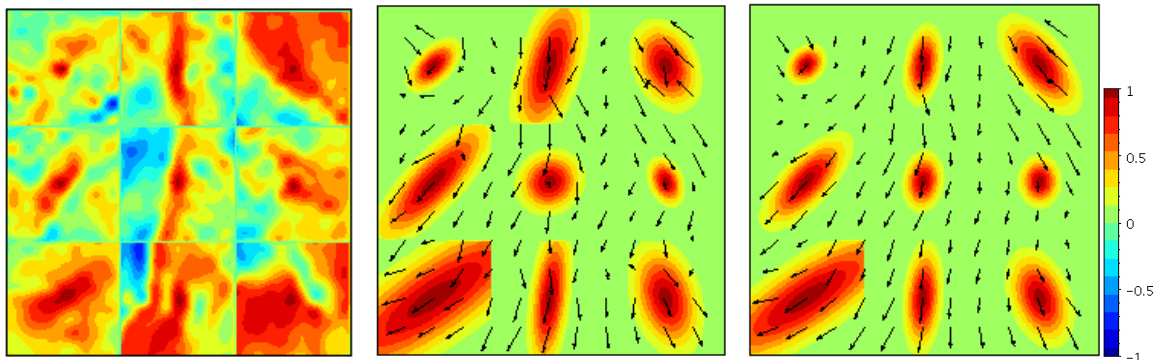

(a) Sample (b) BPB (c) Filtered BPB

Figure: The [BeloPereira and Berre 2006] Tensor for local correlation function

Background Error Modeling: Spatial Deformations

Change of spatial coordinate (deformation, warping, distortion) is a way of achieving anisotropic correlations.
Possibly consistent with Kalman Filter Propagation Equations:

$$\mathbf{B} = \mathbf{M}\mathbf{A}\mathbf{M}^{\mathrm{T}} + \mathbf{Q}$$

(especially if advection if predominant in $\mathbf{M}$?)

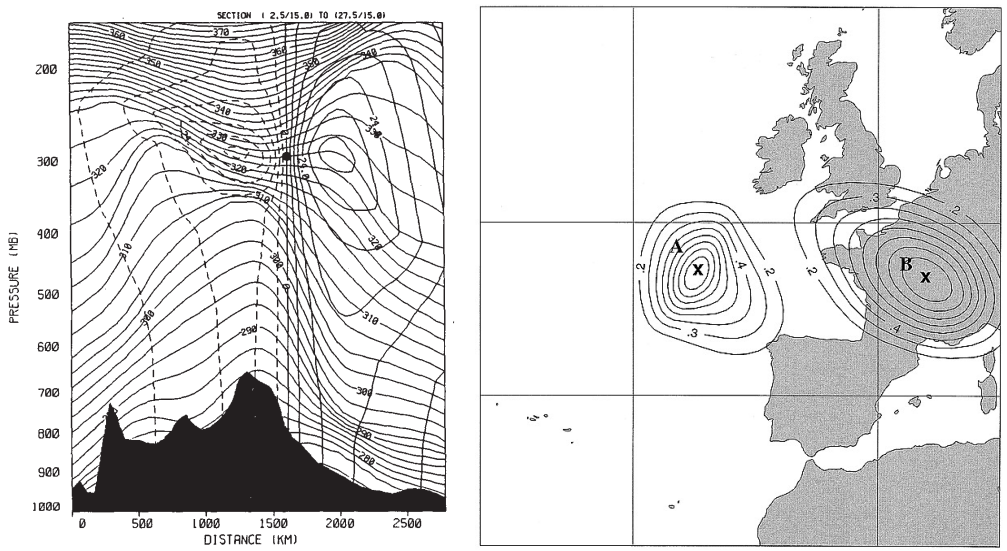

(a) [Benjamin 1989] (b) [Desroziers 1997]

Figure: Single obs test (a) with an isentropic analysis and (b) with a semi-geostrophic transform

Background Error Modeling: Spatial Deformations

Change of spatial coordinate (deformation, warping, distortion) is a way of achieving anisotropic correlations.
Possibly consistent with Kalman Filter Propagation Equations:

$$\mathbf{B} = \mathbf{M}\mathbf{A}\mathbf{M}^{\mathrm{T}} + \mathbf{Q}$$

(especially if advection if predominant in $\mathbf{M}$?)

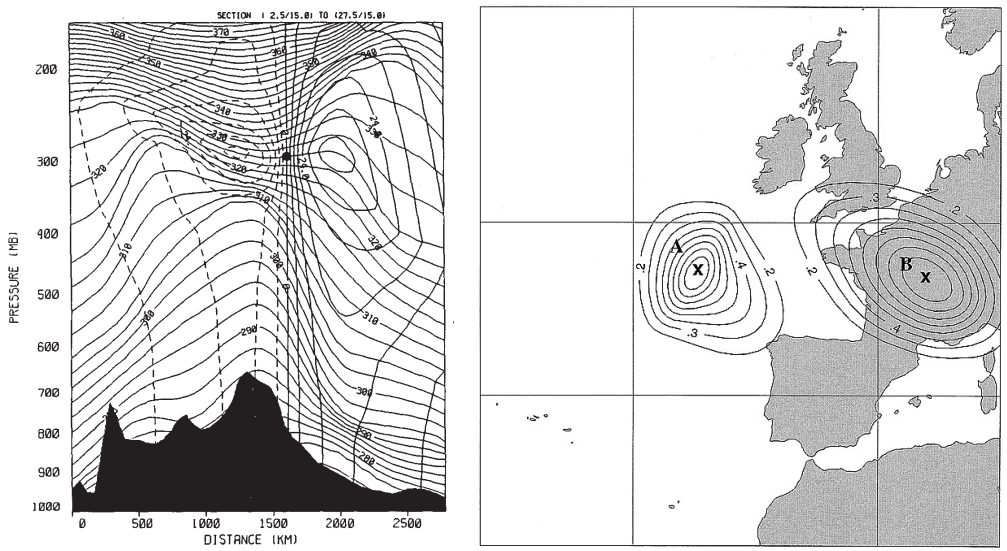

(a) [Benjamin 1989] (b) [Desroziers 1997]

Figure: Single obs test (a) with an isentropic analysis and (b) with a semi-geostrophic transform

Huge drawback: here, the deformation is (almost) arbitrary.

Estimating Deformation for correlation modeling

The goal is to find a grid deformation that reduce the correlation model to an isotropic and/or stationary one (that may be modeled with Fourier or recursive filter approaches).

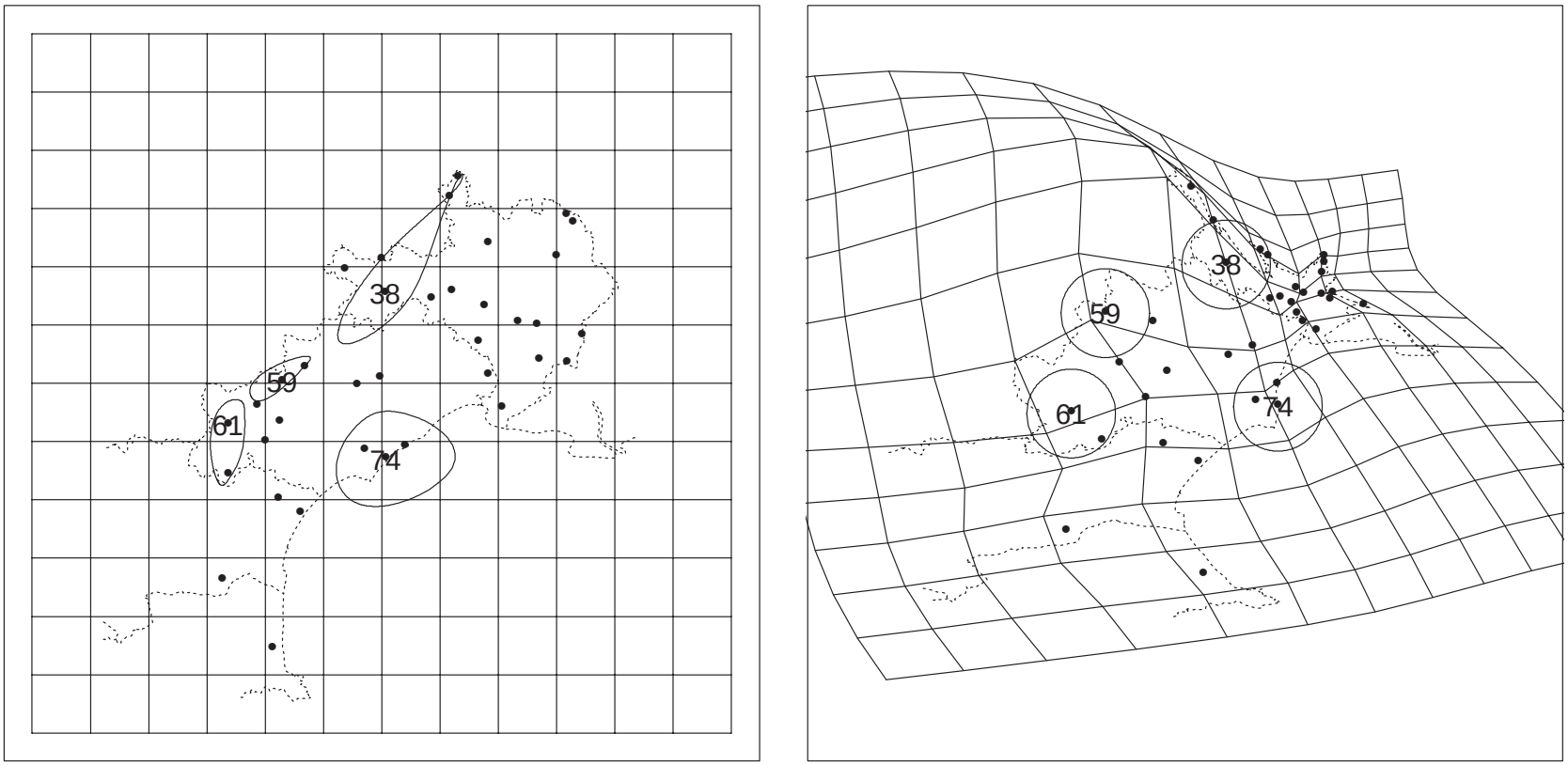

Figure: Geographic map of rainfall monitoring sites in the Languedoc-Roussillon region (Southern France) with 0.9 correlation contours [Sampson et al. 2003].

BPB Tensor may not be sufficient (?)

Imagine that at each grid point, the local correlation function is given by a BPB ellipse. Then the local grid transformation (Jacobian) must be

$$J_D = \begin{pmatrix} \frac{\partial D_1}{\partial x_1} & \frac{\partial D_1}{\partial x_2} \\ \frac{\partial D_2}{\partial x_1} & \frac{\partial D_2}{\partial x_2} \end{pmatrix} = \begin{pmatrix} \cos(\theta) & -\sin(\theta) \\ \sin(\theta) & \cos(\theta) \end{pmatrix} \begin{pmatrix} \frac{L_a}{L} & 0 \\ 0 & \frac{L_b}{L} \end{pmatrix}$$

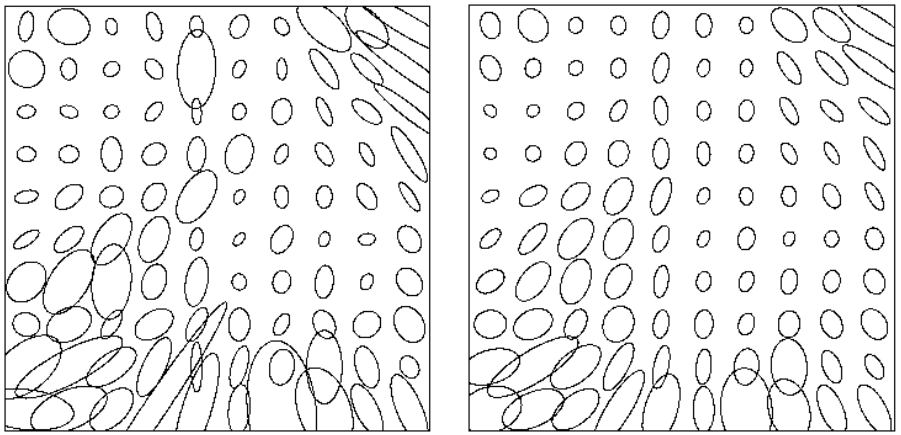

(a) Raw BPB (b) Filtered BPB

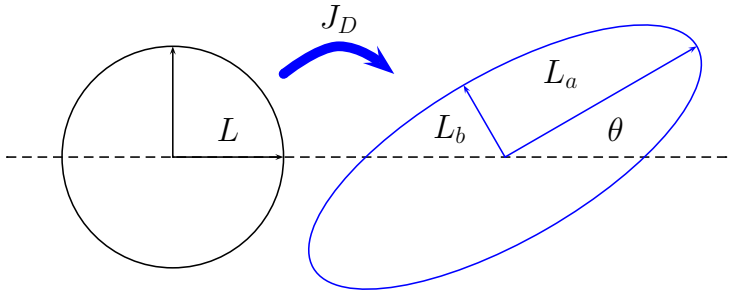

(c) J_D

Problem may arise from the fact that we only know θ modulo π, that it may not be continuous and that we may not verify Schwartz condition.

Computer Vision: The "Shape from Texture" Problem

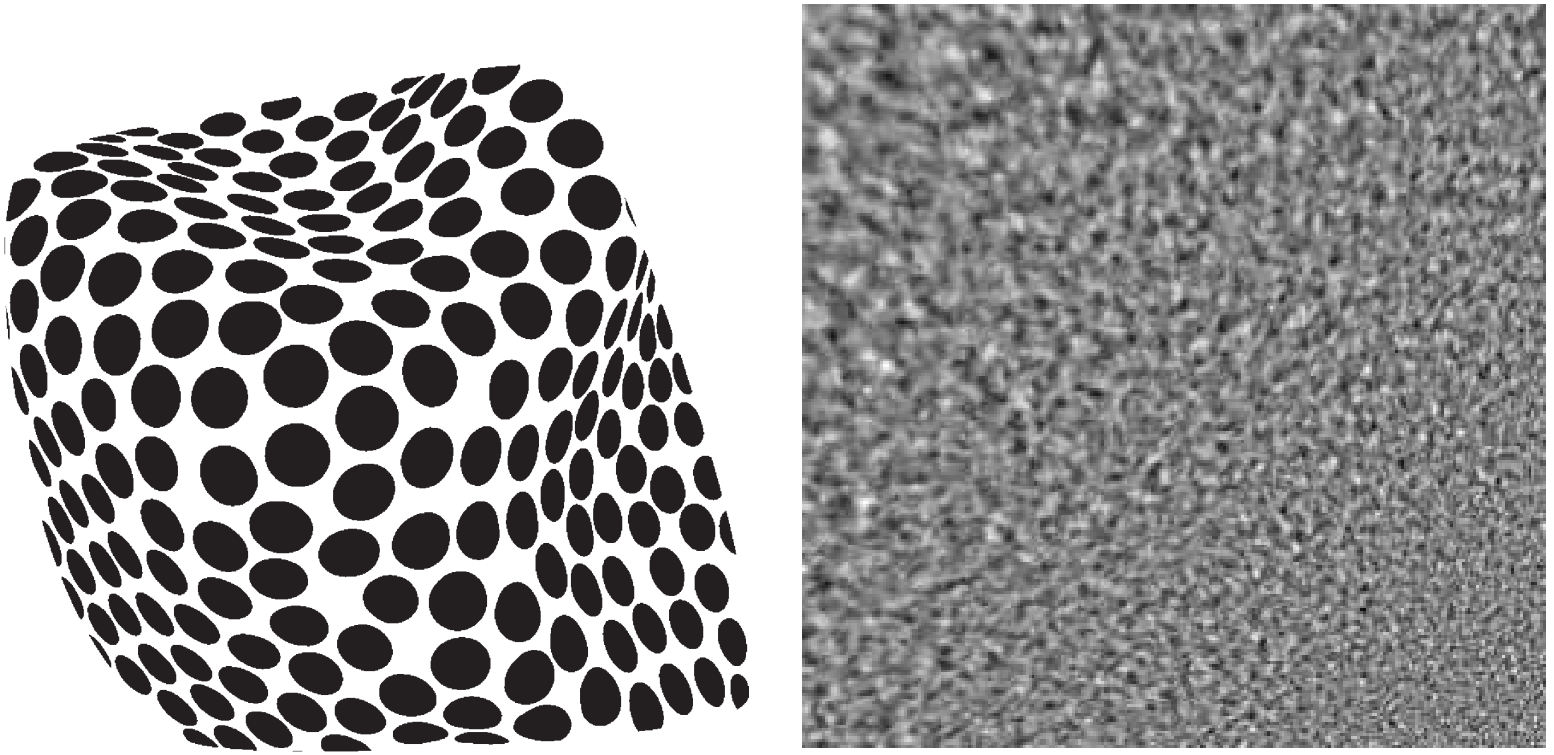

(a) [Todd et al 2005] (b) From M. Clerc's PhD (1999)

Figure: Effect of surface distortion and perspective on stationary "texture".

What is the definition of a texture? How to recover the shape of the surface from the measurement of texture gradients?

The Wavelet Migration Property

Consider a warped random process $F = R\big(d(x)\big)$ where R is wide-sense stationary. A local analysis of F may be performed with wavelets:

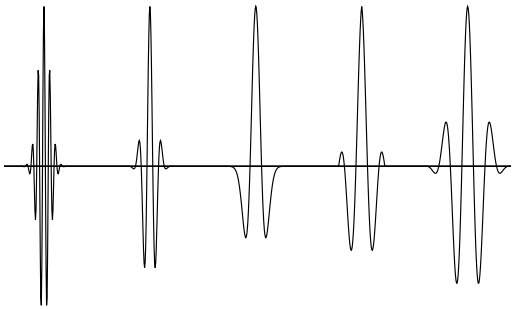

$$\psi_{u,s}(x) = \frac{1}{s}\psi\left(\frac{x-u}{s}\right)$$

The inner product $< F, \psi_{u,s} >$ is a continuous wavelet coefficient and the scalogramm is

$$w(u,s) = \mathbb{E}\{|| < F, \psi_{u,s} > ||^2\}$$

The Wavelet Migration Property states that

$$w(u,s) = \mathbb{E}\{|| < F, \psi_{u,s} > ||^2\} \approx \mathbb{E}\{|| < R, \psi_{d(u),d'(u)s} > ||^2\}$$

The Texture Gradient Equation

The Texture Gradient links the warping d with the apparent velocity of w in the $(u, \log s)$ plane:

$$\big(1 + \mathcal{O}(s)\big)\frac{\partial w(u,s)}{\partial u} - \frac{d''(u)}{d'(u)}\frac{\partial w(u,s)}{\partial \log s} = 0$$

Applying the "Shape from Texture" solution to 1D correlation model I

We follow 1D test-bed suggested by [Pannekoucke et al 2007], where correlations are stretched by a C2.4 Schmidt transform.

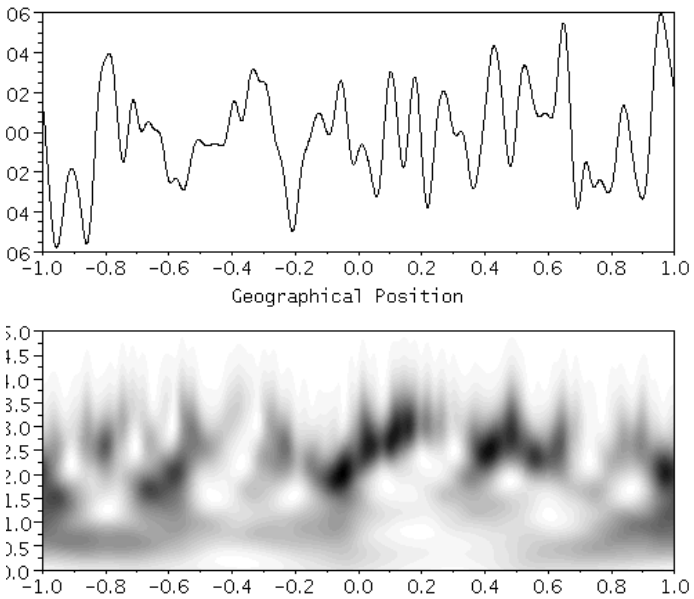

(a) R and w

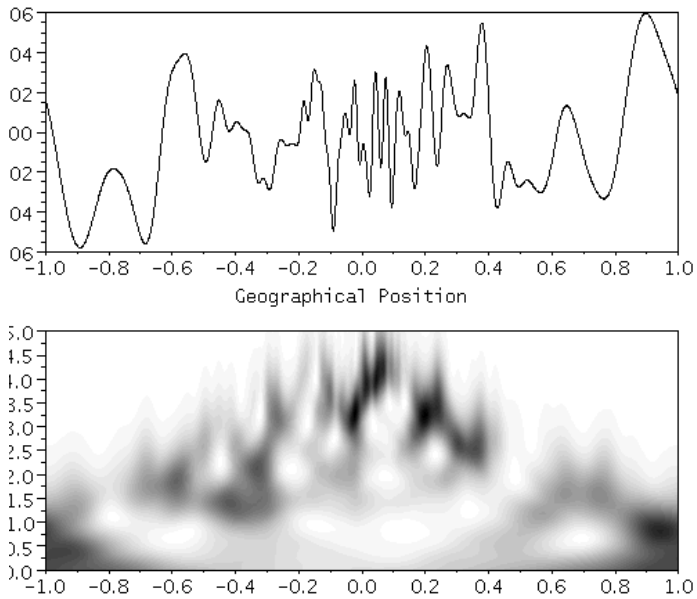

(b) F and w

Need to use spatial convolution h_Δ to get robust results.

$$h_\Delta \star \left(\left(1 + \mathcal{O}(s)\right) \frac{\partial w(u,s)}{\partial u} - \frac{d''(u)}{d'(u)} \frac{\partial w(u,s)}{\partial \log s} \right) = 0$$

Applying the "Shape from Texture" solution to 1D correlation model II

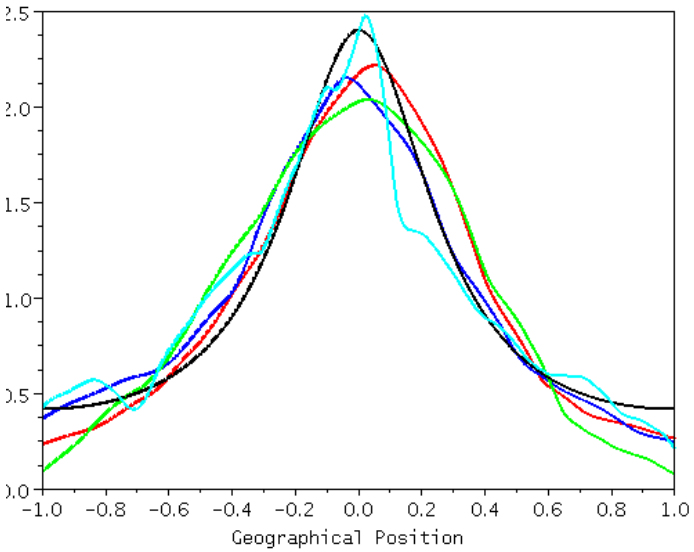

(a) d' and $\widehat{d'}$

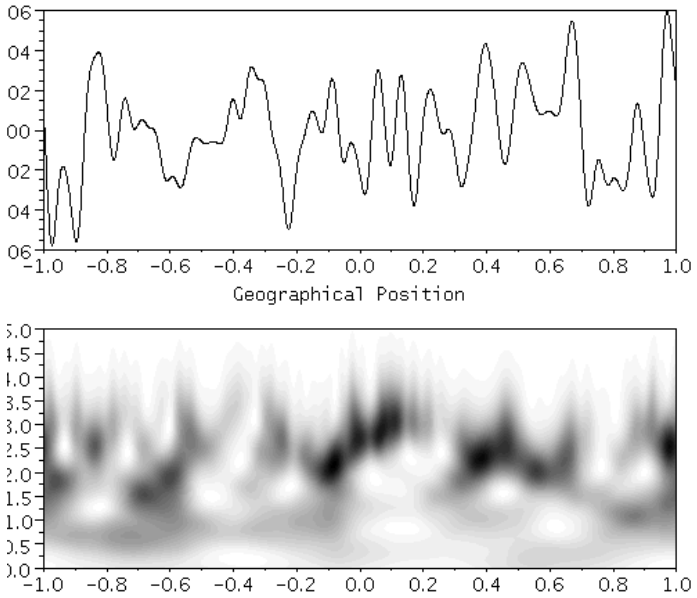

(b) $\widehat{D}^{-1}F$ and w

Figure: Results of the algorithm for different wavelets (Spline-Box, Sombrero and Gabor), for one realization of F. Spatial convolution is $\Delta = N/3$ ($\Delta = N/10$)

It is possible to estimate d given appropriate boundary conditions.

$$\widehat{d(u)} = \int_0^u \exp\left(\int_0^x \frac{\widehat{d''(v)}}{d'(v)} dv + A \right) dx + B$$

Thus, hybrid deformation-wavelet/curvelet/RF... is possible.

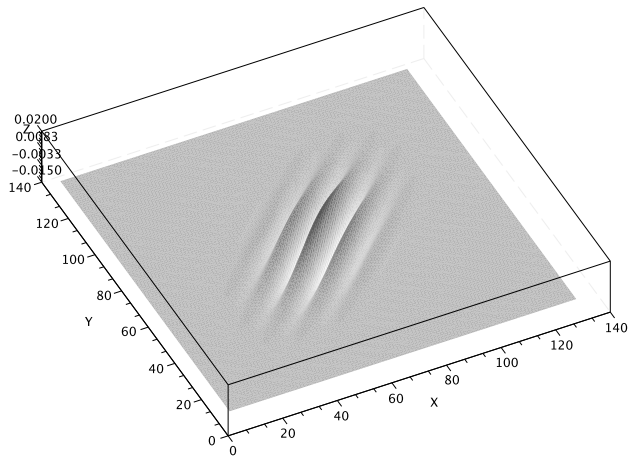

Figure: A warplet

Anisotropy is one goal, so directional wavelets are required.

$$S = \begin{pmatrix} s_{11} & s_{12} \\ s_{21} & s_{22} \end{pmatrix}$$

$$\psi_{\mathbf{u},S} = \det S^{-1} \psi\big(S^{-1}(\mathbf{x} - \mathbf{u})\big)$$

The variance of the warplet coefficient is a function of 6 parameters $\mathbf{u}, S$:

$$w(u, S) = \mathbb{E}\{|| < F, \psi_{\mathbf{u},S} > ||^2\}$$

Yes, there is a warplet migration property and a texture gradient equation (but you probably don't want to see the equations [Clerc and Mallat 2002]). The texture gradient is

$$J_D^{-1} \partial_{u_k} J_D$$

Applying the "Shape from Texture" solution to 2D correlation model II

2D case is different because

- texture gradient has to be estimated in a higher dimensional space, requiring evaluation of w and its partial derivatives with many warping matrices S
- it is not trivial to integrate the deformation from the texture gradient.

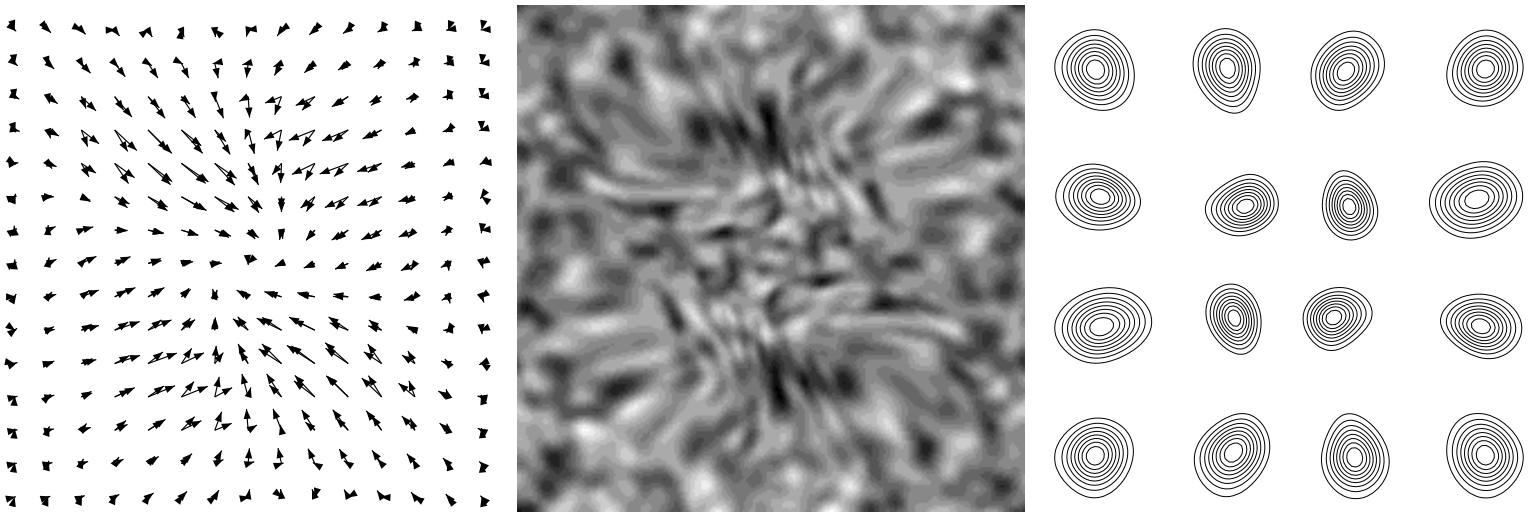

(a) $\mathbf{d}$ and $\widehat{\mathbf{d}}$ (b) Warped process F (c) Warped Correlation

Conclusion

Amplitude-Position Data Assimilation

Amplitude-Position Data Assimilation incorporates displacement fields into the control variable as a way of (better?) dealing with coherent structures (tropical cyclones, clouds, water vapor and PV...).
Most studies assume that displacement is locally regular, and incorporate smoothness penalty terms. These Tikhonov Regularizations are equivalent to inverse covariance operators.
Tools to study this problem have been developed during my stay @NCAR.

Conclusion

Amplitude-Position Data Assimilation

Amplitude-Position Data Assimilation incorporates displacement fields into the control variable as a way of (better?) dealing with coherent structures (tropical cyclones, clouds, water vapor and PV...).
Most studies assume that displacement is locally regular, and incorporate smoothness penalty terms. These Tikhonov Regularizations are equivalent to inverse covariance operators.
Tools to study this problem have been developed during my stay @NCAR.

Background Error Modeling

Spatial Deformations are being studied as an alternative way of designing inhomogeneous anisotropic spatial correlations.
Need to compare different approaches for computing deformations.
So far, only idealized data with "shape from texture" approach.

Conclusion

Amplitude-Position Data Assimilation

Amplitude-Position Data Assimilation incorporates displacement fields into the control variable as a way of (better?) dealing with coherent structures (tropical cyclones, clouds, water vapor and PV...).
Most studies assume that displacement is locally regular, and incorporate smoothness penalty terms. These Tikhonov Regularizations are equivalent to inverse covariance operators.
Tools to study this problem have been developed during my stay @NCAR.

Background Error Modeling

Spatial Deformations are being studied as an alternative way of designing inhomogeneous anisotropic spatial correlations.
Need to compare different approaches for computing deformations.
So far, only idealized data with "shape from texture" approach.

Visit at NCAR founded by the AFWA/ACAPS Project.
Warm thanks to Tom Auligné. Questions welcome!

References I

Auligné T., A. Lorenc, Y. Michel, T. Montmerle, A. Jones, M. Hu, J. Dudhia

Toward a New Cloud Analysis and Prediction System
BAMS, doi: 10.1175/2010BAMS2978.1, 2010

Beezley, J. D. and J. Mandel

Morphing ensemble Kalman filters.
Tellus, **60**, 131–140, 2008

Belo-Pereira, M. and L. Berre

The use of an ensemble approach to study the backgound error covariances in a global NWP model.
Mon. Weather Rev., **134**, 2466–2489, 2006

Benjamin, S. G.

An isentropic meso-alpha scale analysis system and its sensitivity to aircraft and surface observations.
Mon. Wea. Rev., **117**, 1586-1603, 1989.

D. Béréziat and I. Herlin

Solving ill-posed image processing problems using data assimilation.
Numerical Algorithms, 2010

Berre, L.

Estimation of Synoptic and Mesoscale Forecast Error Covariances in a Limited-Area Model.
Mon. Wea. Rev., **128**, 644-667., 2000.

References II

N. Bormann, S. Saarinen, G. Kelly, et J.-N. Thépaut.

The spatial structure of observation errors in atmospheric motion vectors from geostationary satellite data.

Mon. Weather Rev., 131:706–718, 2003.

Chen, Y. and C. Snyder

Assimilating vortex position with an ensemble Kalman filter.

Mon. Weather Rev., **135**, 1828–1845, 2007

M. Clerc and S. Mallat

The Texture Gradient Equation for Recovering Shape from Texture

IEEE Transactions on Pattern Analysis and Machine Intelligence, **24**,4,536-549 2002.

M. Clerc and S. Mallat

Estimating deformations of stationary processes

Ann. Statist. Volume **31**, Number 6 2003, 1772-1821.

Deckmyn, A., L. Berre

A Wavelet Approach to Representing Background Error Covariances in a Limited-Area Model

Mon. Wea. Rev., **133**, 1279-1294.

Deckmyn, A.

A Complex Wavelet representation of Error Covariances in ALADIN 3d-Var

Krakow, April 13, 2010

Desroziers, G.

A Coordinate Change for Data Assimilation in Spherical Geometry of Frontal Structures.

Mon. Wea. Rev., **125**, 3030-3038, 1997.

References III

D. C. Dowell and D.J. Stensrud

Ensemble forecasts of severe convective storms
24th Conference on Severe Local Storms, 2008.

Fournier A.

Development of Wavelet Methodology for WRF Data Assimilation
NCAR Seminar/Symposium, 2010

Horn, B.K.P., and Schunck, B.G.,

Determining Optical Flow,
AI(17), No. 1-3, August 1981, pp. 185-203

N G Kingsbury:

Complex wavelets for shift invariant analysis and filtering of signals
Journal of Applied and Computational Harmonic Analysis, vol 10, no 3, May 2001, pp. 234-253.

Lawson, W. and J. Hansen

Alignment error models and ensemble-based data assimilation.
Mon. Weather Rev., **133**, 1687–1709, 2005

Michel, Y. and T. Auligné

Inhomogeneous Background Error Modeling and Estimation over Antarctica
Mon. Wea. Rev., **138**, 2229–2252, 2010.

Michel, Y. and F. Bouttier

Automated tracking of dry intrusions on satellite water vapour imagery and model output.
Quart. Journal of the Royal Met. Society, **132**, 2257–2276, 2006

References IV

Michel, Y.

Data Assimilation of Tropopause Height Using Dry Intrusion Observations
Mon. Weather Rev., **138**, 101–122, 2009

T. Nehrkorn, R.N. Hoffman, Ch. Grassotti, J-F. Louis

Feature calibration and alignment to represent model forecast errors: Empirical regularization
Quart. Journal of the Royal Met. Society, **129**, 587A, 195-218, 2003.

D.S. Oliver

Calculation of the Inverse of the Covariance
Mathematical Geology, **30**, Number 7, 911-933, 1998.

O. Pannekoucke, L. Berre, G. Desroziers

Filtering properties of wavelets for local background-error correlations
Quarterly Journal of the Royal Meteorological Society Volume 133, Issue 623, pages 363-3379, January 2007 Part B

Purser, R., W. Wu, D. Parrish, and N. Roberts

Numerical Aspects of the Application of Recursive Filters to Variational Statistical Analysis. Part II: Spatially Inhomogeneous and Anisotropic General Covariances
Mon. Wea. Rev., **131**, 1536–1548, 2003.

Ravela, S., K. Emanuel, and D. McLaughlin

Data assimilation by field alignment
Physica D, **230**, 127–145, 2007

P. D. Sampson, D. Damian, P. Guttorp, T. Gneiting

Nonstationary spatial covariance modeling via spatial deformation
SAMSI Multiscale Workshop, Feb. 2003

References V

Tarantola, A.

Inverse Problem Theory and Methods for Model Parameter Estimation
Society for Industrial and Applied Mathematics ISBN 0-89871-572-5, 2005.

Todd, J.T. Thaler, L. and Dijkstra, T.M.H.

The effects of field of view on the perception of 3D slant from texture
Vision Research **45**, 12, 1501-1517, 2005

Wu, W., R. Purser, and D. Parrish

Three-Dimensional Variational Analysis with Spatially Inhomogeneous Covariances
Mon. Wea. Rev., **130**, 2905-2916, 2002.

C. Yang and S. Ravela

Spectral Control of Diffeomorphic Field Alignment for Deformation Invariant Matching
Proc. ICCV, pp. 1303-1310, Kyoto, Japan, 2009.